iScience

CellPress
OPEN ACCESS

Article

Targeting an essential *Plasmodium* cold shock protein to block growth and transmission of malaria parasite

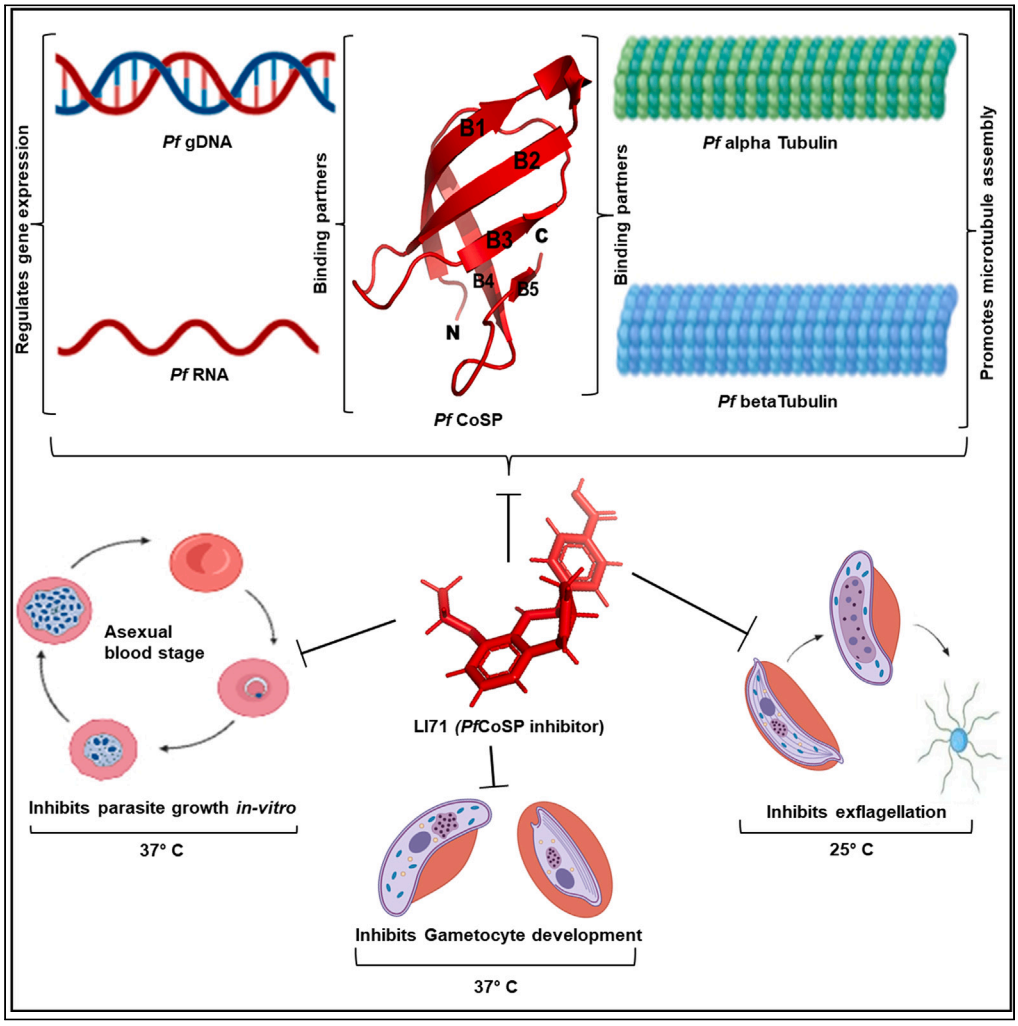

Ankita Behl, Rumaisha Shoaib, Fernando De Leon, ..., Prakash Chandra Mishra, Christoph Arenz, Shailja Singh

shailja.jnu@gmail.com

Highlights

*Pf*CoSP exhibits nucleic acid binding properties and regulates gene expression

*Pf*CoSP binds *Pf* α/β tubulin and promotes microtubule assembly

LI71 interacts with *Pf*CoSP and inhibits its binding with DNA and tubulin

LI71 inhibits asexual and sexual development of malaria parasite

Behl et al., iScience *26*, 106637
May 19, 2023
https://doi.org/10.1016/j.isci.2023.106637

iScience

CellPress
OPEN ACCESS

Article

Targeting an essential *Plasmodium* cold shock protein to block growth and transmission of malaria parasite

Ankita Behl,[1,6] Rumaisha Shoaib,[1,2,6] Fernando De Leon,[3] Geeta Kumari,[1,7] Monika Saini,[1,4,7] Evanka Madan,[1,7] Vikash Kumar,[1] Harshita Singh,[1] Jyoti Kumari,[4] Preeti Maurya,[1] Swati Garg,[1] Prakash Chandra Mishra,[5] Christoph Arenz,[3] and Shailja Singh[1,8,*]

SUMMARY

Cold shock proteins are characterized by the presence of one or more cold shock domains that bestow them with nucleic acid binding ability. Although cold shock proteins are well characterized in bacteria, plants and humans, there is no information on their existence and role in malaria parasite. Here, we have identified and delineated the function of a cold shock protein of *Plasmodium falciparum* (*Pf*) '*Pf*CoSP'. We demonstrate that *Pf*CoSP exhibits nucleic acid binding properties and regulates gene expression. *Pf*CoSP promotes microtubule assembly by interacting with *Pf* α/β tubulin. We identified a human cold shock protein LIN28A inhibitor 'LI71' as a binding partner of *Pf*CoSP which inhibited *Pf*CoSP–DNA and α/β tubulin interactions and, also inhibited the development of asexual blood stages and gametocyte stage of malaria parasite. Because *Pf*CoSP is essential for parasite survival, characterization of its interacting partners may form the basis for development of future anti-malarials.

INTRODUCTION

All organisms face changing environmental conditions and have the potential to cope with different types of stress environments. One of the most typical stresses that all living organisms experience is cold shock. To combat with the adverse effects of low temperature, cold shock proteins are expressed in bacteria, plants and humans that play a crucial role in acquiring cold tolerance.[1–5] Cold shock proteins harbor one or more cold shock domain that forms the defining characteristic of cold shock protein family. Cold shock domain has DNA and RNA binding motifs that make cold shock proteins regulate critical processes inside the cell including transcription, translation and splicing. Cold shock proteins are known to destabilize secondary structures in target RNA which in turn allow efficient transcription and translation.[3,6]

Cold shock proteins were first discovered in bacteria when a drop in temperature induced the expression of a cold shock protein A (CspA) in *Escherichia coli*.[7,8] *E. coli* encodes 9 cold shock protein genes (*CspA* to *CspI*) that encode highly conserved family of structurally related proteins with a molecular mass of approximately 7.4 kDa.[9] Bacterial Csps possess the characteristic cold shock domains necessary for interaction with single-stranded RNA and DNA.[10–14] The moderately well-conserved nucleic acid binding motifs RNP1 (K/R-G-F/Y-G/A-F-V/I-X-F/Y) and RNP2 (L/I-F/Y-V/I-G/K-N/G-L) promote this protein-DNA/RNA interaction.[15,16] Structural studies on bacterial cold shock proteins indicate that they possess an OB (oligonucleotide/oligosaccharide-binding) fold that comprises 5 antiparallel β strands forming a Greek-key β-barrel.[17]

In humans, eight members of cold shock proteins exist that are encoded by genes namely YBX1, YBX2, YBX3, CARHSP1, CSDC2, CSDE1, LIN28A, and LIN28B.[18] YBX1, YBX2, YBX3 encode Y-box binding protein-1 (YB-1), DNA binding protein A (DbpA) and C (DbpC) respectively and comprise Y-box binding protein family.[18] YB-1 interacts with both DNA and RNA and is involved in several critical processes including mRNA splicing, mRNA translation, DNA replication and repair.[19–22] Calcium-regulated heat-stable protein 1 (CARHSP1) is known to bind with tumor necrosis factor (TNF) mRNA[23] whereas PIPPin (encoded by CSDC2) binds precisely to the 3′-UTR ends of both histone H1 and H3.3 mRNAs.[24] Role of

[1]Special Centre for Molecular Medicine, Jawaharlal Nehru University, New Delhi, India

[2]Department of Biosciences, Jamia Millia Islamia, New Delhi, India

[3]Institute for Chemistry, Humboldt University, Berlin, Germany

[4]Department of Life Sciences, Shiv Nadar University, Greater Noida, Uttar Pradesh, India

[5]Department of Biotechnology, Guru Nanak Dev University, Amritsar, India

[6]These authors contributed equally

[7]These authors contributed equally

[8]Lead contact

*Correspondence: shailja.jnu@gmail.com

https://doi.org/10.1016/j.isci.2023.106637

CARHSP1 is associated with TNF stabilization within P-bodies and exosomes[23] whereas function of PIPPin is linked with the negative regulation of histone variant synthesis in the developing brain.[24] Unr (upstream of N-ras) is another human cold shock protein (encoded by CSDE1) that is involved in translational reprogramming.[25] Another developmentally important cold shock protein expressed in humans is Lin28 whose function is to regulate translation of mRNAs that control metabolism, pluripotency and timing of development.[26]

Cold shock proteins are also well characterized in plants like wheat, rice and *Arabidopsis thaliana* and are known to perform several functions like regulating flowering time, embryo and fruit development and also help plants in acquiring freezing tolerance.[27] Radkova et al. identified 4 cold shock protein genes in wheat that were further classified into three classes.[28] Expression of class I and class II proteins is upregulated during seed and flower development whereas class III wheat cold shock protein (27 kDa) is expressed only during seed development.[28] Four cold shock proteins (AtCSP1-CSP4) from *A. thaliana* are known to interact with RNA, single and double-stranded DNA. Among these, AtCSP3 (At2 g17870) is essential for acquiring freezing tolerance[29] whereas AtCSP2 and AtCSP4 are involved in regulating development processes.[30,31] Chaikam and Karlson identified two cold shock proteins in rice (OsCSP1 and OsCSP2) whose role is more related with developmental processes as compared to cold tolerance.[32]

Although the roles of cold shock proteins in bacteria, plants, and humans are well understood, there is no information on the presence and role of cold shock proteins in *Plasmodium falciparum*. Our search in Plasmodb database[33] identified a single cold shock gene in malaria parasite. The PhenoPlasm database[34] and piggyBac essentiality screen[35] indicated that *Pf*CoSP is essential for survival of the parasite inside the human host. This underscores its significance in parasite biology and makes it an attractive candidate for development of antimalarials. In the present study, we have attempted to elucidate the function of *Pf*CoSP in malaria parasite. Our data suggest that *Pf*CoSP regulates gene expression and interacts with α/β tubulin possibly to promote microtubule assembly. Also, *Pf*CoSP binds with LIN28 inhibitor 'LI71' that inhibits *Pf*CoSP-DNA and *Pf*CoSP-α/β tubulin interactions and, showed antiplasmodial activity against *Pf*3D7 and chloroquine resistant strain *Pf*RKL-9. *Pf*CoSP expression was upregulated at low temperature, suggesting its prominent role during cold stress faced by the parasite on entering to mosquito host. Overall, our data implicate the role of *Pf*CoSP in growth and development of malaria parasite on cold stress.

RESULTS

Domain organization, cloning, expression and purification of *Pf*CoSP

Sequence analysis and domain organization using Blastp depicted that *Pf*CoSP is 150 amino acid long and has a characteristic N-terminal cold shock domain that contains a DNA binding site and an RNA binding motif[36] (Figure 1Ai). We next explored the presence of *Pf*CoSP homologues in other species using organism-specific Blastp search in *E. coli*, higher plants and *Homo sapiens*. Multiple sequence alignment of cold shock domain of *Pf*CoSP with its homologs revealed that predicted residues comprising the DNA binding site and RNA binding motif in *Pf*CoSP are moderately conserved among its homologues in bacteria (CspG), plants (*Capsicum annuum*, *Hibiscus syriacus*, *Manihot esculenta*) and humans (LIN28A, CRHSP1, YBX1) (Figure 1Aii). Phylogenetic analysis of *Pf*CoSP with its homologs in other species showing evolutionary distances among them is represented in Figure 1Aiii.

*Pf*CoSP was cloned in pET-28a(+) (T7 promoter based plasmid), and expressed in the soluble form in *E. coli* BL21 (DE3) cells with a 6X hexahistidine tag. *Pf*CoSP was purified using Ni-NTA affinity chromatography (Figure 1B). Identity of recombinant *Pf*CoSP was checked by western blotting using antihistidine antibodies (Figure S1A). Male BALB/c mice were used to produce polyclonal antisera against *Pf*CoSP, and testing on a crude extract of *E. coli* BL21 (DE3) transformed with its cloned plasmid confirmed the antisera's specificity (Figure S1B).

*Pf*CoSP exhibits nucleic acids binding properties

*Pf*CoSP carries DNA and RNA binding domains. Therefore, we used pull-down assays and gel retardation assay to test nucleic acid binding properties of *Pf*CoSP. Cellulose beads containing immobilized calf thymus ssDNA and dsDNA were used to perform nucleic acid hybridization assay. 1 μg *Pf*CoSP was mixed with cellulose matrix and incubated at 4°C for 30 min. Bead pellet was extensively washed and boiled in 1X SDS-PAGE sample loading dye before loading on 15% SDS-PAGE. Band for *Pf*CoSP was detected in boiled beads sample, indicative of its interaction with both ssDNA and dsDNA (Figure 1C). No protein band was

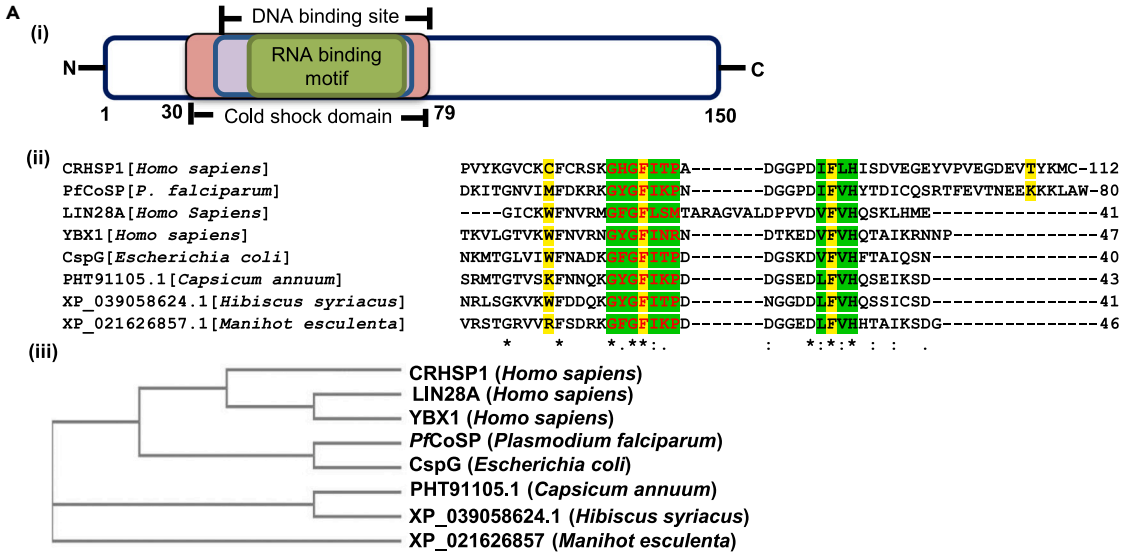
A
(i)
DNA binding site
RNA binding motif
N
C
1
30
Cold shock domain
79
150
(ii)
CRHSP1[Homo sapiens] PVYKGVCKCFCRSKGHGETTA-------DGGPDIFLHISDVEGEYVPVEGDEVTYKMC-112
PfCoSP[P. falciparum] DKITGNVIMFDKRKGTGETTKN-------DGGPDIFVHYTDICQSRTFEVTNEEKKKLAW-80
LIN28A[Homo Sapiens] ----GICKWFNVRMGFGFISM-TARAGVALDPPVDVFVHQSKLHME----------41
YBX1[Homo sapiens] TKVLGTVKWFNVRNGYGFINR-------DTKEDVFVHQTAIKRNNP----------47
CspG[Escherichia coli] NKMTGLVIWFNADKGFGFITP-------DGSKDVFVHFTAIQSN----------40
PHT91105.1[Capsicum annuum] SRMTGTVSKFNNQKGYGFIKP-------DGSEDLFVHQSEIKSD----------43
XP_039058624.1[Hibiscus syriacus] NRLSGKVKWFDDQKGYGFITP-------NGGDDLFVHQSSICSD----------41
XP_021626857.1[Manihot esculenta] VRSTGRVVRFSDRKGFGFIKP-------DGGEDLFVHHTAIKSDG----------46
(iii)
CRHSP1 (Homo sapiens)
LIN28A (Homo sapiens)
YBX1 (Homo sapiens)
PfCoSP (Plasmodium falciparum)
CspG (Escherichia coli)
PHT91105.1 (Capsicum annuum)
XP_039058624.1 (Hibiscus syriacus)
XP_021626857 (Manihot esculenta)
B
kDa
Marker
PfCoSP
70
55
37
25
15
~18.5 kDa
CBB stained SDS-PAGE
C
dsDNA
ssDNA
kDa
Marker
+PfCoSP
wash
+BSA
BSA wash
+PfCoSP
wash
+BSA
wash
90
70
55
37
25
15
10
CBB stained SDS-PAGE
D
PfgDNA + + + + + + PfRNA
PfCoSP - + - - + - PfCoSP
BSA - - + - - + BSA
1% agarose gel
E
Interaction between PfCoSP and gDNA
Dose-response curve
K_D = 0.137 nM
Fnorm [‰]
690
685
680
675
670
1.0E-11 1.0E-10 1.0E-09 1.0E-07 1.0E-06 1.0E-05
Ligand concentration
MST signal
Relative fluorescence[-]
1
0.9
0.8
0.7
0 5 10 15 20
Time [s]
F
Interaction between PfCoSP and RNA
Dose-response curve
K_D= 8.88 nM
Fnorm [‰]
890
888
886
884
882
880
1.0E-12 1.0E-11 1.0E-10 1.0E-09 1.0E-07 1.0E-06
Ligand concentration
MST signal
Relative fluorescence[-]
1
0.9
0.8
0.7
0 5 10 15 20
Time [s]

Figure 1. *Pf*CoSP exhibits DNA and RNA binding ability

(A i) Schematic representation of predicted domains and motifs of *Pf*CoSP.

(A ii) Multiple sequence alignment of *Pf*CoSP with its homologs in *Escherichia coli*, *Homo sapiens* and plants (*Capsicum annuum*, *Hibiscus syriacus*, *Manihot esculenta*). Residues marked with yellow are predicted residues involved in DNA binding and those highlighted in green and marked with red are predicted to be involved in RNA binding.

(A iii) Phylogenetic analysis of *Pf*CoSP with its homologs in other species showing evolutionary distances among them.

(B) SDS-PAGE showing recombinant purified *Pf*CoSP tagged with 6x-Histidine stained with Coomassie Brilliant Blue (CBB).

(C) *Pf*CoSP-DNA interaction using pull down assay. *Pf*CoSP and negative control BSA were incubated with single stranded (ss) DNA oligomer/double stranded (ds) DNA immobilized cellulose beads in a pull down assay. Elutes and washes from the assay were loaded on 15% SDS-PAGE as depicted.

(D) Gel retardation assay showing *Pf*CoSP-nucleic acid interaction. Left panel: Agarose gel (1%) showing *Pf*CoSP-DNA binding. Right panel: Agarose gel (1%) showing *Pf*CoSP-*Pf*RNA binding. Samples are depicted with + and – above each lane.

(E and F) Interaction studies of *Pf*CoSP with *Pf*gDNA (E) and *Pf*RNA (F) using Microscale Thermophoresis (MST). Purified recombinant *Pf*CoSP was labeled with RED-NHS Lysine dye followed by titration with varying concentrations of *Pf* gDNA and *Pf* RNA. Dose-response curves generated K_d of 0.137 nM and 8.88 nM for *Pf*CoSP-gDNA interactions, respectively.

detective in negative control where beads were incubated with BSA (Figure 1C). Nucleic acid binding properties of *Pf*CoSP was also analyzed using gel retardation assay. *Pf*CoSP was incubated separately with *Pf* gDNA and RNA and subjected to agarose gel electrophoresis. Retardation in migration of nucleic acids was observed suggesting that *Pf*CoSP binds with both DNA and RNA (Figure 1D). Negative control where BSA was incubated with DNA and RNA did not show any shift in an agarose gel on incubation with *Pf* gDNA and RNA (Figure 1D), highlighting the specificity of the assay.

To further validate the binding, kinetic analysis of one-to-one interaction of purified recombinant *Pf*CoSP with *Pf* gDNA and *Pf* RNA was carried out using NanoTemper Monolith NT.115 instrument. Here labeled *Pf*CoSP was titrated against varying concentrations of *Pf* DNA and *Pf* RNA. Figures 1E and 1F shows dose-response curves and MST (Microscale Thermophoresis) signals for *Pf*CoSP- *Pf* gDNA and *Pf*CoSP- *Pf* RNA binding respectively. K_d for *Pf*CoSP-*Pf* gDNA and *Pf*CoSP-*Pf* RNA binding was observed to be 0.137 nM and 8.88 nM respectively, suggesting strong binding of *Pf*CoSP for DNA and RNA.

*Pf*CoSP interacts with cytoskeleton proteins alpha tubulin and beta tubulin

A proposed model for the coordinated cellular responses in mammalian cells on exposure to mild hypothermia cold-shock was reported by Al-Fageeh et al. In the model, cold shock proteins can link transcription and translation via interactions with target mRNAs and the cytoskeleton.[37] In light of the above fact, we examined the binding of *Pf*CoSP with components of cell cytoskeleton viz. α and β tubulin using *in vitro* and *in vivo* assays. Preliminary screening was performed using semi-quantitative ELISA assays that depict significant binding of *Pf*CoSP with α and β tubulin in a concentration dependent manner. Binding of *Pf*CoSP with α and β tubulin showed saturation at higher concentrations (Figure 2A).

We also performed kinetic analysis of one-to-one interaction of purified recombinant *Pf*CoSP with α and β tubulin using NanoTemper Monolith NT.115 instrument. Here labeled *P. falciparum* α and β tubulins were titrated against varying concentrations of *Pf*CoSP (ranging from 0.0061 μM to 20 μM). Figures 2B and 2C shows dose-response curves and MST signals for *Pf*CoSP-α/β tubulin binding. In the MST data, the response amplitude can be negative or positive, depending on the exact influence of ligand binding on the target MST signal. The response amplitude is negative for α tubulin + *Pf*CoSP binding as the MST signal of the complex (*Pf*CoSP + α tubulin) is lower than that of the target alone (*Pf*CoSP) and positive for β tubulin + *Pf*CoSP as the MST signal of the complex (*Pf*CoSP + beta tubulin) is higher than that of target (*Pf*CoSP) alone. K_d for *Pf*CoSP-α/β tubulin binding was observed to be 210 nM and 6.49 μM respectively, suggesting significant binding of *Pf*CoSP with α and β tubulin. Plots representing MST data of *Pf*CoSP with BSA as negative control are represented in Figure S2.

In vivo co-immunoprecipitation assays followed by western blot analysis also validated the above results. *Pf*CoSP specific antisera was coupled to aminolink plus coupling resin, and used to pull down α and β tubulin from parasite culture. Elutes from the assay were probed by western blot analysis using anti-α and β tubulin antibodies separately. Although a distinct band corresponding to α and β tubulin eluted from *Pf*CoSP specific antisera coupled beads, none was observed for preimmune sera linked beads (negative control) (Figures 2Di and 2Diii). Reverse co-immunoprecipitation assays further validated the interaction where anti-α and β tubulin antibodies were coupled to aminolink plus coupling resin separately, and used to pull down *Pf*CoSP from parasite culture. Elutes from the assay were probed by western blot analysis

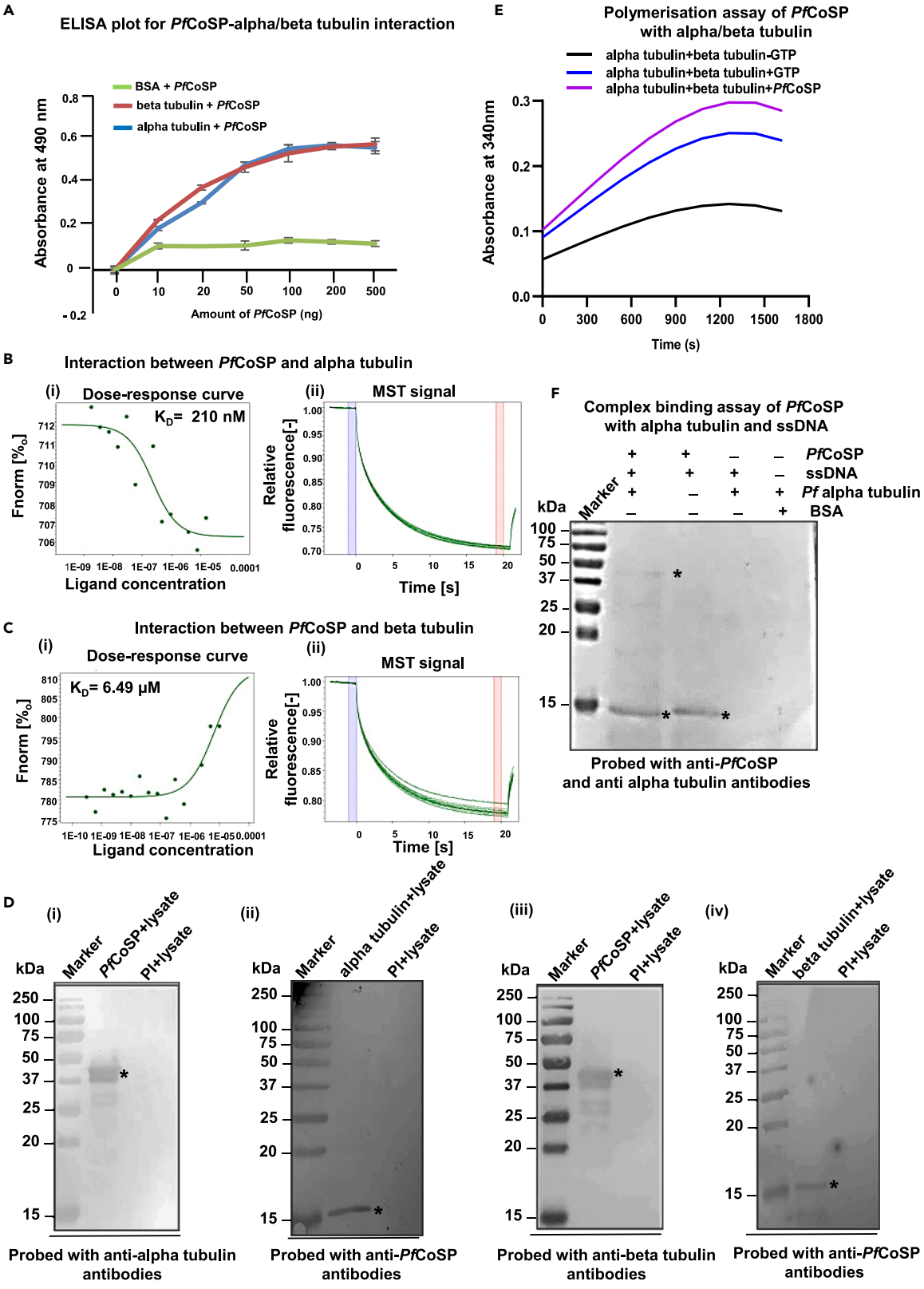
A
ELISA plot for PfCoSP-alpha/beta tubulin interaction
BSA + PfCoSP
beta tubulin + PfCoSP
alpha tubulin + PfCoSP
Absorbance at 490 nm
Amount of PfCoSP (ng)
E
Polymerisation assay of PfCoSP with alpha/beta tubulin
alpha tubulin+beta tubulin-GTP
alpha tubulin+beta tubulin+GTP
alpha tubulin+beta tubulin+PfCoSP
Absorbance at 340nm
Time (s)
B
Interaction between PfCoSP and alpha tubulin
(i) Dose-response curve
K_D= 210 nM
Fnorm [‰]
Ligand concentration
(ii) MST signal
Relative fluorescence[-]
Time [s]
C
Interaction between PfCoSP and beta tubulin
(i) Dose-response curve
K_D= 6.49 µM
Fnorm [‰]
Ligand concentration
(ii) MST signal
Relative fluorescence[-]
Time [s]
F
Complex binding assay of PfCoSP with alpha tubulin and ssDNA
PfCoSP
ssDNA
Pf alpha tubulin
BSA
kDa
Marker
Probed with anti-PfCoSP and anti alpha tubulin antibodies
D
(i)
Marker
PfCoSP+lysate
PI+lysate
Probed with anti-alpha tubulin antibodies
(ii)
Marker
alpha tubulin+lysate
PI+lysate
Probed with anti-PfCoSP antibodies
(iii)
Marker
PfCoSP+lysate
PI+lysate
Probed with anti-beta tubulin antibodies
(iv)
Marker
beta tubulin+lysate
PI+lysate
Probed with anti-PfCoSP antibodies

Figure 2. Interaction of *Pf*CoSP with α and β tubulin and complex formation of *Pf*CoSP with ssDNA and tubulin

(A) Semi-quantitative ELISA. Concentration-dependent binding curves of *Pf*CoSP with α and β tubulin where y-axis represents absorbance at 490 nm and x-axis denotes amount of *Pf*CoSP. Error bars represent standard deviation among three replicates. Blue and red line depicts *Pf*CoSP-α tubulin and *Pf*CoSP-β tubulin binding, respectively whereas green depicts BSA as negative control.

(B and C) Interaction studies of *Pf*CoSP with α tubulin (B) and β tubulin (C) using MST. Labeled *P. falciparum* α and β tubulins were titrated against varying concentrations of *Pf*CoSP. Dose-response curves were generated that resulted in K_d values of 210 nM and 6.49 μM for *Pf*CoSP-α tubulin and *Pf*CoSP- β tubulin interactions respectively.

(D) Co-immunoprecipitation assay. *Pf*CoSP (D i, iii), α tubulin (D ii) and β tubulin specific antisera (iv) were coupled to aminolink plus coupling resin, and used to pull down α/β tubulin (D i, iii) and *Pf*CoSP (D ii, iv), respectively from parasite culture. Preimmune antisera (PI) was used as a control in each pull down assay. Protein bands are marked with '*'.

(E) *Pf*CoSP promotes microtubule assembly. Graph represents the turbidimetry plot of tubulin assembly in the absence or presence of *Pf*CoSP (10 μM). Purified *Pf* α and *Pf* β tubulins were incubated with *Pf*CoSP and the absorbance at 340 nm was monitored as an indicator of tubulin polymerisation.

(F) Complex binding assays depicting complex formation of *Pf*CoSP with ssDNA and α tubulin. Recombinant *Pf*CoSP was incubated with the cellulose beads with immobilized single stranded calf thymus DNA and post washing allowed to bind with α tubulin. Elutes from the assay were analyzed by western blot analysis using specific polyclonal antisera against *Pf*CoSP and α tubulin simultaneously. Samples are depicted with + and – above each lane. Elute from single-stranded DNA oligomer immobilized cellulose beads incubated with *Pf*CoSP were loaded as a positive control. Elutes from beads incubated with α tubulin and elutes from beads incubated with BSA followed by α tubulin were loaded as negative control. Protein bands are marked with '*'.

using anti-*Pf*CoSP antibodies separately. A distinct band corresponding to *Pf*CoSP eluted from α and β tubulin specific antisera coupled beads, whereas none was observed for preimmune sera linked beads (negative control) (Figures 2Dii and 2Div).

*Pf*CoSP promotes microtubule assembly *in vitro* and binds with RNA and tubulin simultaneously to form a complex

Because *Pf*CoSP binds with α and β tubulin, we tested whether *Pf*CoSP has any effect on tubulin polymerization by performing *in vitro* tubulin polymerization assay. Purified *Pf* α and *Pf* β tubulins were incubated with *Pf*CoSP and the absorbance at 340 nm was recorded as an indicator of tubulin polymerization. The increase in absorbance demonstrated enhanced microtubule assembly in the presence of *Pf*CoSP (Figure 2E). These data suggest that *Pf*CoSP has the capability to promote microtubule assembly.

Our previous results showed that *Pf*CoSP binds to both RNA and *Pf* tubulin. In light of this, we tested its potential to attach with both simultaneously to form a complex using cellulose beads with immobilized single stranded calf thymus DNA. Recombinant *Pf*CoSP was incubated with the beads, and after washing allowed to bind with α tubulin. Elutes from the experiment were examined by immunublotting using specific polyclonal antisera against *Pf*CoSP and α tubulin simultaneously. Distinct bands of *Pf*CoSP and α tubulin eluted from beads were observed whereas no band was detected where beads were first incubated with BSA followed by α tubulin showing the specificity of the assay (Figure 2F). *Pf*CoSP was incubated to beads as positive control. These data suggest that *Pf*CoSP binds with RNA and α tubulin simultaneously to form a complex. No band for β tubulin was observed from *Pf*CoSP bound ssDNA beads (Figure S2iii).

In silico binding studies of *Pf*CoSP with LI71 and their interaction using Microscale Thermophoresis

We performed extensive literature survey to look for an inhibitor for a cold shock protein. We found a molecule named L171 that directly binds the cold shock domain of a human cold shock protein 'LIN28' to suppress its activity against let-7 in leukemia cells and embryonic stem cells.[38] Multiple sequence alignment of cold shock domain of *Pf*CoSP (Query cover 52%) shares 30.3% sequency identity with LIN28A that suggests significant similarity between the proteins (Figure 1Aii). Therefore, we tested this inhibitor for binding with *Pf*CoSP and inhibiting its interaction with α/β tubulin. NMR spectra of LI71 is represented in Figures S3–S6 and its synthetic scheme is shown in Figure S7. Preliminary analysis of interaction was performed by docking modeled structure of cold shock domain of *Pf*CoSP with LI71 using Patchdock.[39] Modeling details of *Pf*CoSP are described in our previous report.[36] We observed that LI71 binds well into the cavity of *Pf*CoSP with a binding energy of −64.01 kJ/mol (Figure 3A). Analysis of docked structure using PrankWeb webserver[40] gave detail analysis of binding site. Residues of *Pf*CoSP predicted to form the pocket for LI71 and possibly involved in interaction include I46, V57, H58, Y59, T60, D61, R66, T67, F68, A79, W80 and N81 (Figure 3A). Out of these, we have shown earlier that H58 and Y59 are predicted to form maximum number of interactions with B-DNA and RNA.[36]

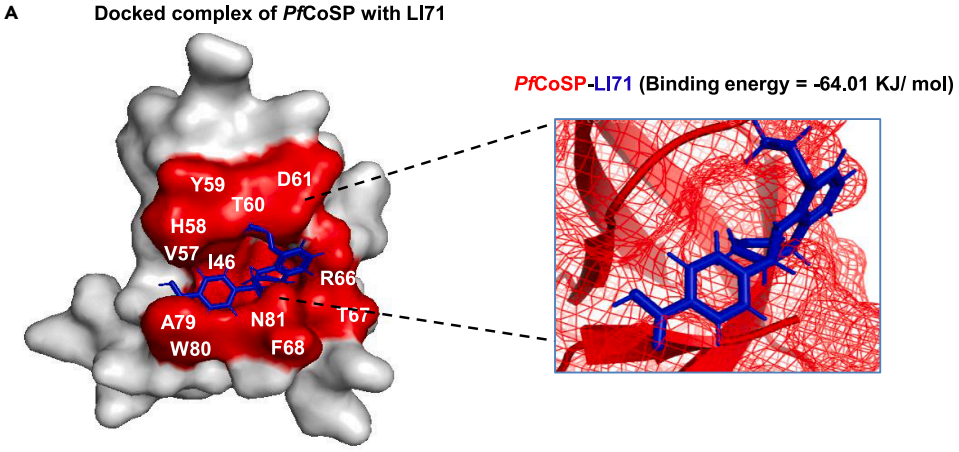
A
Docked complex of PfCoSP with LI71
PfCoSP-LI71 (Binding energy = -64.01 KJ/ mol)
Y59
D61
T60
H58
V57
I46
R66
A79
N81
T67
W80
F68

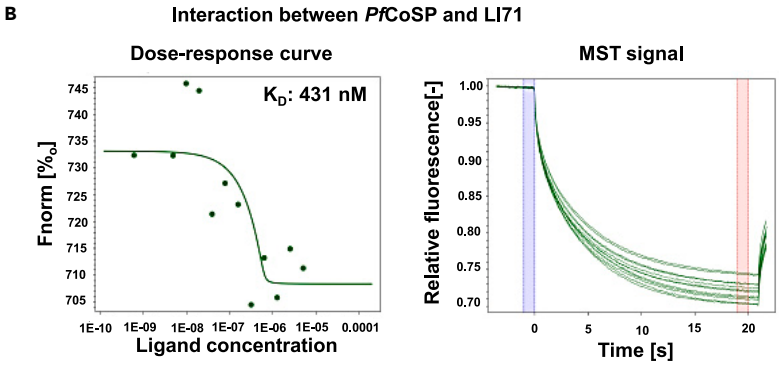
B
Interaction between PfCoSP and LI71
Dose-response curve
MST signal
K_D: 431 nM
Fnorm [‰]
Ligand concentration
Relative fluorescence[-]
Time [s]

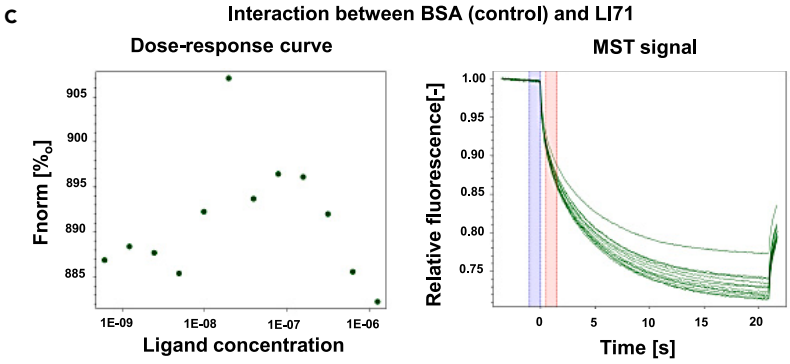
C
Interaction between BSA (control) and LI71
Dose-response curve
MST signal
Fnorm [‰]
Ligand concentration
Relative fluorescence[-]
Time [s]

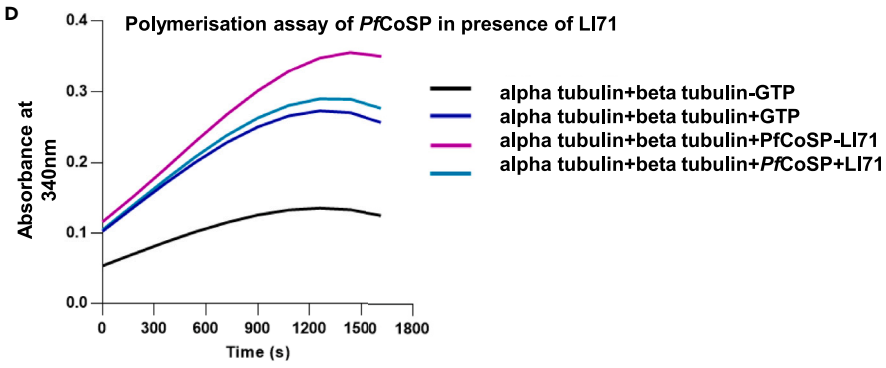
D
Polymerisation assay of PfCoSP in presence of LI71
Absorbance at 340nm
Time (s)
alpha tubulin+beta tubulin-GTP
alpha tubulin+beta tubulin+GTP
alpha tubulin+beta tubulin+PfCoSP-LI71
alpha tubulin+beta tubulin+PfCoSP+LI71

Figure 3. *In silico* binding of *Pf*CoSP with LI71 using docking studies and validation of *Pf*CoSP-L171 interaction using MST

(A) Left panel: Docked complex of *Pf*CoSP with LI71. Gray represents *Pf*CoSP whereas blue denotes LI71. Residues of *Pf*CoSP predicted to be involved in LI71 binding are highlighted in red and marked with white. Right panel: Zoomed image showing the enlarged view of *Pf*CoSP-LI71 binding site.

(B) Interaction studies of *Pf*CoSP with LI71 using MST. Labeled *Pf*CoSP was titrated against varying concentrations of LI71. Dose-response curve (left panel) was generated that resulted in K_d value of 431 nM for *Pf*CoSP-LI71 interaction. (C) Plots represents MST data of BSA with LI71 as a negative control.

(D) Effect of LI71 on *Pf* microtubule assembly in presence of *Pf*CoSP. Graph represents the turbidimetry plot of tubulin assembly in the presence and absence of LI71. Purified *Pf* α- and *Pf* β-tubulins were incubated with *Pf*CoSP in the presence and absence of LI71 and the absorbance at 340 nm was monitored as an indicator of tubulin polymerization.

To further validate *Pf*CoSP-LI71 interaction, kinetic analysis of one-to-one interaction of purified recombinant *Pf*CoSP with L171 was carried out using NanoTemper Monolith NT.115 instrument. *Pf*CoSP was labeled and LI71 was serially diluted with maximum concentration at 20 μM. Figure 3B shows dose-response curve and MST signal for *Pf*CoSP-L171 binding. K_d for *Pf*CoSP-LI71 binding was observed to be 431 nM. Plots representing MST data of BSA with LI71 as a negative control is shown in Figure 3C.

Effect of LI71 on *Pf* microtubule assembly in the presence of *Pf*CoSP

Our previous results showed that *Pf*CoSP enhance tubulin polymerization by binding with *Pf*tubulin, therefore we investigated whether LI71 has any effect on *Pf*CoSP function of microtubule assembly by using *in vitro* tubulin polymerization assay. Here, purified *Pf* α and *Pf* β tubulins were incubated with *Pf*CoSP in the presence and absence of LI71 and the absorbance at 340 nm was recorded as an indicator of tubulin polymerization. Our results showed that in the presence of LI71, tubulin assembly was inhibited (Figure 3D). These data suggest that LI71 hinders *Pf*CoSP in promoting microtubule assembly.

LI71 inhibits *Pf*CoSP-DNA and alpha/beta tubulin interactions

MST can be employed to perform competition experiment owing to several advantages it poses. The technique is label-free and site-specific resulting in reliable information regarding the ability of a compound to interrupt the protein-protein interaction.[41] We employed this technique to test whether LI71 can inhibit *Pf*CoSP-DNA and α/β tubulin interactions. Here, interaction between recombinant *Pf*CoSP and gDNA was established through evaluation of thermophoretic mobility of moieties in a temperature gradient via Monolith (NanoTemper Technologies, Munich, Germany). Thiazole orange (TO) labeled gDNA on titration with recombinant *Pf*CoSP revealed a decreasing MST signal (F_{norm} [‰] starting at 830 units, increasing to 778 units) with increasing concentration of *Pf*CoSP yielding a sigmoidal curve giving a K_d value of 78.9 nM (Figure 4A). This low K_d value represents a strong interaction between gDNA and *Pf*CoSP. Further, competition assay was performed to evaluate competitive property of LI71 to interfere the interaction between gDNA and *Pf*CoSP. An increasing MST signal was obtained displaying F_{norm} level at 844 units increasing to 960 units with K_d 455 nM with increasing concentration of LI71 (Figure 4B). Overall, it suggests a significant interaction of LI71 with *Pf*CoSP displacing the labeled gDNA based on the MST signals. Thus, based on our findings we can interpret LI71 as a molecule competing with gDNA to bind with *Pf*CoSP.

To test the effect of LI71 on *Pf*CoSP-α/β tubulin interactions, labeled α and β tubulin were titrated against serially diluted *Pf*CoSP followed by analyses with Monolith NT.115 instrument. In case of interaction of α tubulin with *Pf*CoSP, a decreasing MST signal (F_{norm} [‰] starting at 712 units, decreasing to 706 units) was observed with increasing concentration of *Pf*CoSP yielding a sigmoidal curve giving a K_d value of 274 nM. This low K_d value represents a strong interaction between α tubulin with *Pf*CoSP. However, the competition experiment performed with compound LI71 as a competing molecule interfering with the interaction of α tubulin-*Pf*CoSP displayed F_{norm} level at 790 units increasing to 835 units with Kd 12.65 μM while increasing concentration of the compound (Figure 4C). This suggests a significant binding of LI71 with *Pf*CoSP displacing the labeled α tubulin based on the MST signals.

Similarly, interaction of β tubulin with *Pf*CoSP in the presence of LI71 was also analyzed. Concentration of labeled β tubulin was kept constant and titrated against serially diluted *Pf*CoSP. On observation, β tubulin also displayed interaction with *Pf*CoSP with K_d value 7.92 μM with F_{norm} starting from 785 units and increasing to 810 units. When the interaction between β tubulin and *Pf*CoSP was interrupted by increasing concentrations of compound LI71, F_{norm} value decreased from 785 to 710 units, yielding a K_d value of 3.055 μM (Figure 4D). Thus, this change in the MST signal suggests competing property of LI71 against

A

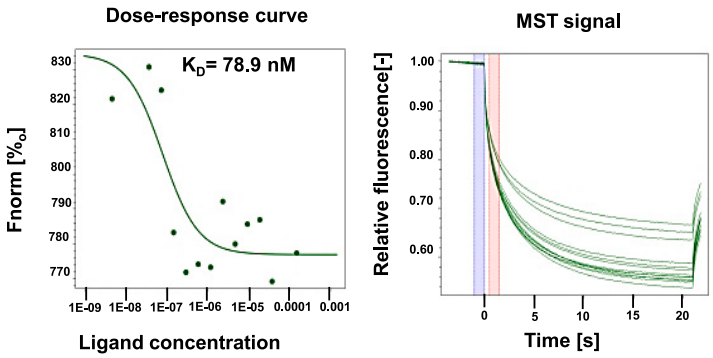
Interaction between PfgDNA and PfCoSP
Dose-response curve
MST signal
K_D= 78.9 nM
Fnorm [‰]
Ligand concentration
Relative fluorescence[-]
Time [s]

B

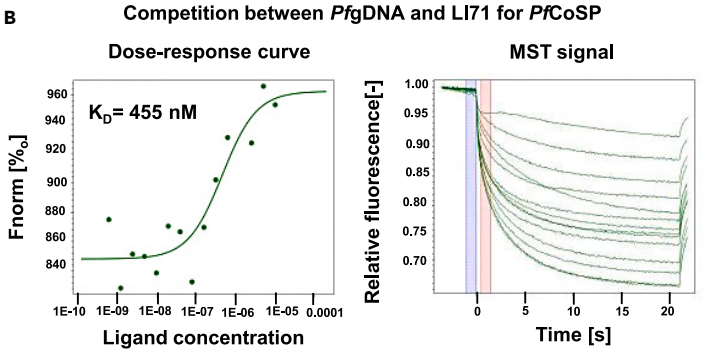
Competition between PfgDNA and LI71 for PfCoSP
Dose-response curve
MST signal
K_D= 455 nM
Fnorm [‰]
Ligand concentration
Relative fluorescence[-]
Time [s]

C

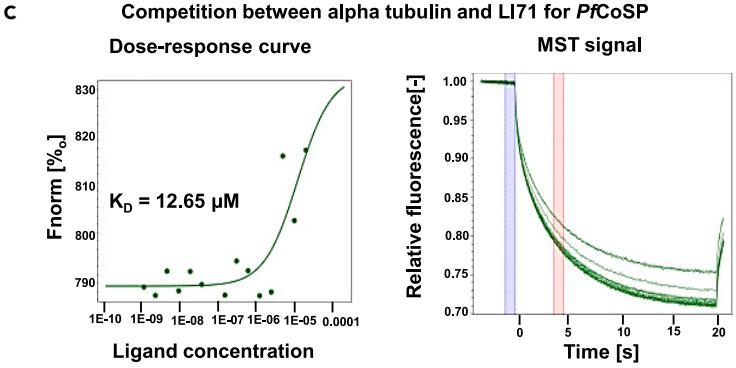
Competition between alpha tubulin and LI71 for PfCoSP
Dose-response curve
MST signal
K_D = 12.65 µM
Fnorm [‰]
Ligand concentration
Relative fluorescence[-]
Time [s]

D

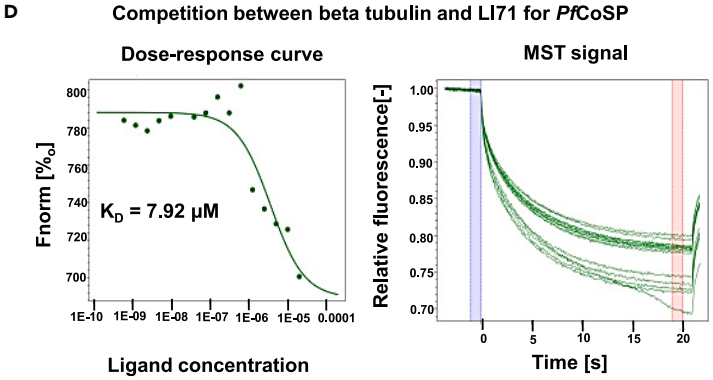
Competition between beta tubulin and LI71 for PfCoSP
Dose-response curve
MST signal
K_D = 7.92 µM
Fnorm [‰]
Ligand concentration
Relative fluorescence[-]
Time [s]

Figure 4. LI71 inhibits *Pf*CoSP-DNA and α/β tubulin interactions

(A) LI71 competes with gDNA to interact with *Pf*CoSP. TO labeled gDNA upon titration with recombinant *Pf*CoSP revealed a decreasing MST signal (F_{norm} [‰] starting at 830 units, increasing to 778 units) with increasing concentration of *Pf*CoSP yielding a sigmoidal curve giving a K_d value of 78.9 nM.

(B) Competition assay was performed to evaluate competitive property of LI71 to interfere the interaction between gDNA and *Pf*CoSP. An increasing MST signal was obtained displaying F_{norm} level at 844 units increasing to 960 units with K_d value of 455 nM with increasing concentration of LI71.

(C and D) LI71 competes with α-tubulin and β-tubulin to interact with *Pf*CoSP. (C) Interaction of α-tubulin with recombinant *Pf*CoSP NHS-Red dye labeled protein (i) was evaluated through MST. The K_d constant of 274 ± 64 nM was obtained in case of interaction of α-tubulin with *Pf*CoSP. A decreasing MST signal (F_{norm} [%] starting at 712 units, decreasing to 706 units) was observed with increasing concentration of *Pf*CoSP yielding a sigmoidal curve. (ii) Competition with compound L171 as a competing molecule interfering with the interaction of α-tubulin-CoSP displayed F_{norm} level at 790 units increasing to 835 units with increasing concentration of the compound.

(D) Similarly, interaction between β-tubulin with *Pf*CoSP (i) was also analyzed. Labeled β-tubulin was titrated against serially diluted *Pf*CoSP. β-tubulin also displayed interaction with *Pf*CoSP with K_d value 7.92 ± 1.43 μM with F_{norm} starting from 785 units and increasing to 810 units yielding a sigmoidal dose-response curve. When the interaction between β-tubulin and *Pf*CoSP was interrupted by increasing concentrations of compound L171, F_{norm} value decreased from 785 to 710 units, yielding a K_d value of 3.055 ± 0.545 μM (ii).

β tubulin to interact with *Pf*CoSP. Overall, based on our findings we can interpret L171 as a compound competing with both the tubulins to bind with *Pf*CoSP.

*Pf*CoSP is expressed in the asexual blood stages and gametocyte stage of parasite

Expression of *Pf*CoSP was assessed at transcript level during the asexual blood stages of *Pf*3D7. Our RT-PCR data showed that *Pf*CoSP expresses at all three stages of asexual blood stage of *Pf*3D7. However, the expression of *Pf*CoSP is higher in trophozoite and schizont stages as compared to ring stage of malaria parasite (Figure 5A). 18S rRNA was used as a loading control to ensure equal loading of cDNA sample.

Expression analysis of *Pf*CoSP during the asexual blood stages was investigated using specific antisera against *Pf*CoSP. Western blot analysis on total protein extracts of mixed stage *Pf* 3D7 infected RBCs detected a single protein band at ~ 17 kDa (Figure 5Bi) for *Pf*CoSP. An identical blot probed with preimmune sera showed no signal (Figure 5Bii). Uninfected erythrocytes lysates were used as negative control in the experiment. The expression of the *Pf*CoSP protein was also explored with different asexual stages of the parasite by western blotting using anti-mice *Pf*CoSP antibodies. *Pf*CoSP was detected in trophozoites [27 to 33 hpi (hours post invasion)] and schizonts (42–48 hpi) but not in ring-stage parasites (15–21 hpi) (Figure 5Ci). As a loading control for the parasite proteins, a parallel western blot experiment was also performed using tubulin specific antibodies (Figure 5Cii). Bar diagram showing plots of intensity measurements of *Pf*CoSP at different asexual stages of parasite is shown in Figure 5Ciii. Here *Pf*CoSP protein levels were quantified at different asexual parasite stages and normalized against α-tubulin protein levels.

We also investigated the change in expression level of *Pf*CoSP on giving temperature treatment in malaria parasite by subjecting schizont stage cultures to 25°C for 6 h. The change was observed by subjecting the samples to immunoblotting and probing with anti-*Pf*CoSP antibodies. The temperature and time of exposure is coherent with the physiological condition that the parasite experiences when it is present in mosquito host. It is important to note that a report on thermal stress and thermoregulation in mosquitoes showed that abdomen temperature of *Anopheles stephensi* depends on the temperature of the host and environment.[42] Abdomen temperature of *A. stephensi* ranges from~ 25°C ($T°_{host}$ = 28°; $T°_{environment}$ = 28°C) to~ 32°C ($T°_{host}$ = 35.5°C, $T°_{environment}$ = 28°C) at the beginning of feeding on an anesthetized mouse. Also, the abdominal temperature decreases of about 2°C during prediuresis.[42] Furthermore, when anopheline mosquitoes ingest a blood meal from an infected host, *Plasmodium* gametocytes present in the erythrocytes undergo differentiation in the mosquito midgut, a process that is highly affected by temperature.[43,44] This cellular differentiation can be mimicked *in vitro* at 25°C.[45] Reports suggest that high temperatures negatively affect early stages of the parasite life cycle and no exflagellation occurs above 30°C.[46] We have therefore used 25°C for mimicking the cold stress condition that parasite experience inside the mosquito host. Furthermore, gametocyte activation involves morphological changes in the parasites that include rounding-up, erythrocyte egress and gamete formation, and these changes occur with approximately 15 min following perception of the environmental signal that include a decrease in temperature which is necessary for gametocyte activation. Parasite development in the midgut of mosquito starts

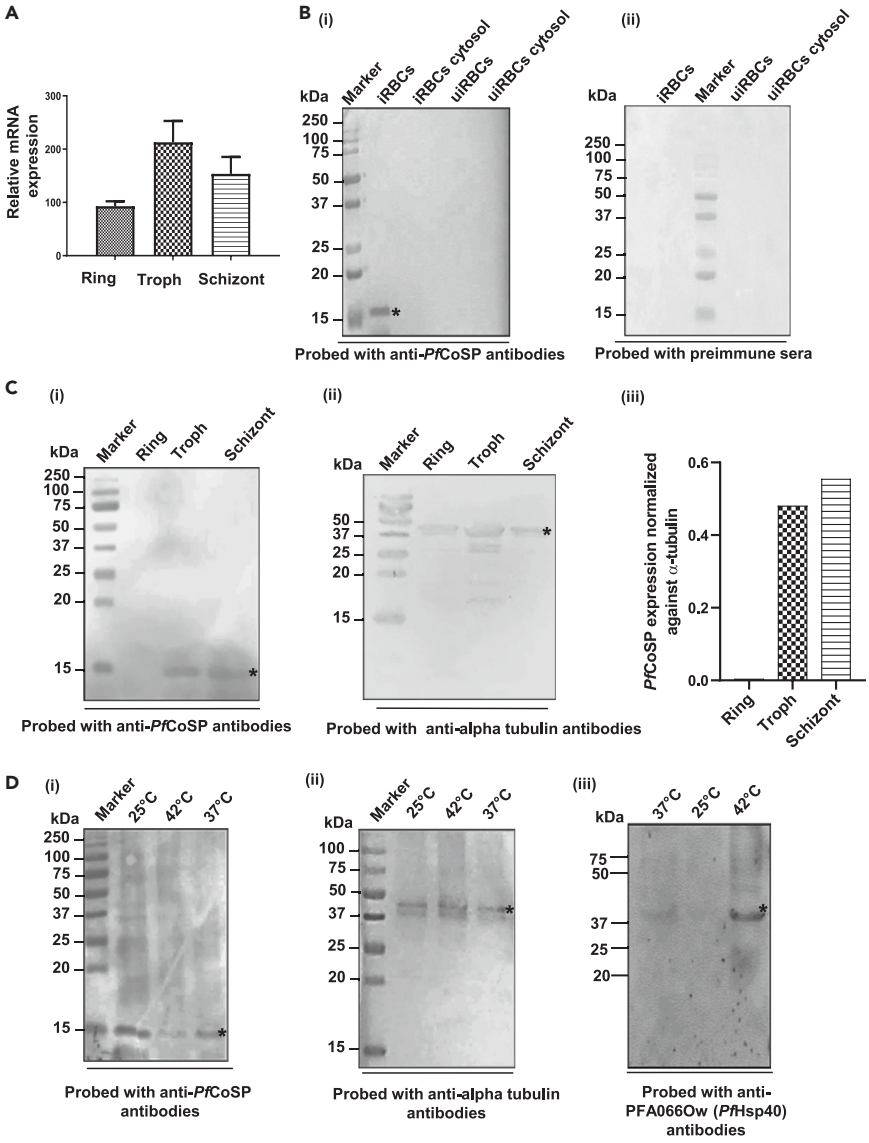

Figure 5. Expression analysis of *Pf*CoSP

(A) Relative expression of *Pf*CoSP at transcript level in asexual blood stages of malaria parasite using RT-PCR. Stages are labeled below the bars. Error bars represent standard deviation among three replicates.

(B i) Detection of *Pf*CoSP (marked with '*') in infected erythrocytes by anti-*Pf*CoSP antibodies. Infected erythrocytes (iRBCs), infected erythrocytes cytosolic fraction (iRBCs cytosol), uninfected erythrocytes (iRBCs) and uninfected erythrocytes cytosolic fraction (uiRBCs cytosol) were loaded on SDS-PAGE and probed with *Pf*CoSP specific antisera. Molecular weight marker is indicated in kDa.

(B ii) Control blot where samples (iRBCs, iRBCs cytosol, iRBCs and uiRBCs cytosol) were probed with preimmune sera as negative control.

(C i) Western blot analysis of stage specific *Pf*3D7 parasite lysates to test *in vivo* expression of *Pf*CoSP. Ring, trophozoite and schizont stage parasite lysate (as mentioned above the lanes on blot) were probed with anti-*Pf*CoSP antibodies followed by secondary antibodies. Molecular weight marker is indicated in kDa. Protein bands are marked with '*'.

(C ii) Blot represents western blot analysis with tubulin specific antibodies as a loading control for the parasite proteins. Ring, trophozoite and schizont stage parasite lysate (as mentioned above the lanes on blot) were probed with anti-tubulin antibodies followed by secondary antibodies. Molecular weight marker is indicated in kDa. Protein bands are marked with '*'.

(C iii) Bar diagram showing plots of intensity measurements of *Pf*CoSP at different asexual stages of parasite. *Pf*CoSP protein levels were quantified at different asexual parasite stages and normalized against α-tubulin protein levels.

Figure 5. *Continued*

(D i) Expression of *Pf*CoSP upregulates on cold stress. Schizont stage culture was treated at 25°C, 37°C, 42° C (as depicted above the lanes) for 6 h and samples were subjected to western blot analysis followed by probing with anti-*Pf*CoSP antibodies. Different temperatures are marked above the lanes on the blot. Molecular weight marker is indicated in kDa. Protein bands are marked with '*'.

(D ii) Blot represents western blot analysis with tubulin specific antibodies as a loading control for the parasite proteins. Schizont stage parasite lysate was probed with anti-tubulin antibodies followed by secondary antibodies. Molecular weight marker is indicated in kDa. Protein bands are marked with '*'.

(D iii) Blot represents western blot analysis with anti-PFA066Ow (*Pf*Hsp40) antibodies as a control for the exposure of parasite to different temperatures (as depicted above the lanes). Protein bands are marked with '*'.

with the activation of the intraerythrocytic gametocytes.[43,47] Post this, the microgamete fertilizes a macrogamete forming a zygote in the mosquito midgut and this event usually takes 1–2 h.[43,48] The midgut phase lasts for approximately 20 h and involves rapid conversion of gametocytes into fertile gametes on activation followed by the formation of motile ookinetes from zygotes.[47] In light of above facts, cold stress was given for 6 h to see its effect on *Pf*CoSP expression. Our results depict that expression level of *Pf*CoSP was higher at 25°C as compared to 37°C and 42°C (Figure 5Di), suggesting its significant role in malaria parasite on cold stress. A parallel western blot was developed with tubulin specific antibodies as a loading control for the parasite proteins (Figure 5Dii). Western blot analysis with anti-PFA066Ow (*Pf*Hsp40) antibodies was also performed as a control for the exposure of parasite to different temperatures (Figure 5Diii).

The expression of *Pf*CoSP during the asexual blood stages of *Pf*3D7 and gametocyte stages of *Pf*RKL9 were investigated by indirect immunofluorescence assays using anti-*Pf*CoSP antibodies. Thin blood smears of mixed stage *Pf*3D7 and *Pf*RKL9 cultures were fixed with methanol and blocked with 5% BSA in PBS. The slides were probed with anti- *Pf*CoSP antibodies (1:200) followed by Alexa Fluor 488 conjugated anti-mice secondary antibodies (1:200). The parasite nuclei were counterstained with DAPI (4′,6′-diamidino-2-phenylindole). Our data showed that *Pf*CoSP is expressed at asexual blood stages as well as gametocyte stages of the parasite (Figure 6A). Expression of *Pf*CoSP was found to be limited to trophozoites and schizonts but not in ring-stage parasites (Figure 6A). These data were consistent with our stage specific detection of *Pf*CoSP in parasite by western blotting. Fluorescence pattern observed for *Pf*CoSP at asexual blood stages was suggestive of its localization to parasite nucleus and cytosol. To confirm its cytosolic localization, co-localization of *Pf*CoSP was performed with a reported *Plasmodium* cytosolic protein, *Pf*NapL. *Pf*CoSP showed significant co-localization with *Pf*NapL that further confirmed its parasite cytosolic localization (Figure 6B).

We also performed co-localization of *Pf*CoSP with α/β tubulin during the asexual stages of *Pf* using protein-specific antibodies on cultured parasites. Our data showed significant overlapping of signals for *Pf*CoSP and α/β tubulin, suggestive of their co-localization (Figure 6C). These results further support interaction of *Pf*CoSP with α and β tubulin.

LI71 inhibits native *Pf*CoSP to interact with DNA and alpha/beta tubulin

Our previous data using MST depicts that LI71 inhibits recombinant *Pf*CoSP to bind with DNA and α/β tubulin. We further performed bead based *Pf*CoSP-DNA pull down assay and co-immunoprecipitation assay to test the effect of LI71 on native *Pf*CoSP to bind with DNA and α/β tubulin respectively. Here cellulose beads with immobilized single and double stranded calf thymus DNA were incubated with parasite lysate treated with and without LI71 at 37°C and 25°C. Bead pellet was washed extensively, boiled in 1X SDS-PAGE sample loading dye followed by western blotting. Samples were probed with anti-*Pf*CoSP antibodies. A distinct band corresponding to *Pf*CoSP was observed where cellulose beads were incubated with parasite lysate not treated with LI71 whereas no band was observed in LI71 treated parasite lysate (Figure 6D). These data further suggest that 'LI71' inhibits the interaction of *Pf*CoSP with DNA/RNA. Similarly, we conducted co-immunoprecipitation assay where *Pf*CoSP specific antisera was coupled to AminoLink Plus Coupling Resin, and used to pull down α and β tubulin from parasite culture treated with and without LI71 at 37°C and 25°C. Elutes from the assay were probed by immunoblotting using anti-α/β tubulin antibodies. We found that a distinct and more prominent band corresponding to α and β tubulin eluted from untreated parasite lysate whereas no band or a less intense band for α and β tubulin appeared for LI71 treated parasite lysate (Figures 6Ei and 6Eii). These data further suggest that 'LI71' hinders the interaction of *Pf*CoSP with α and β tubulin.

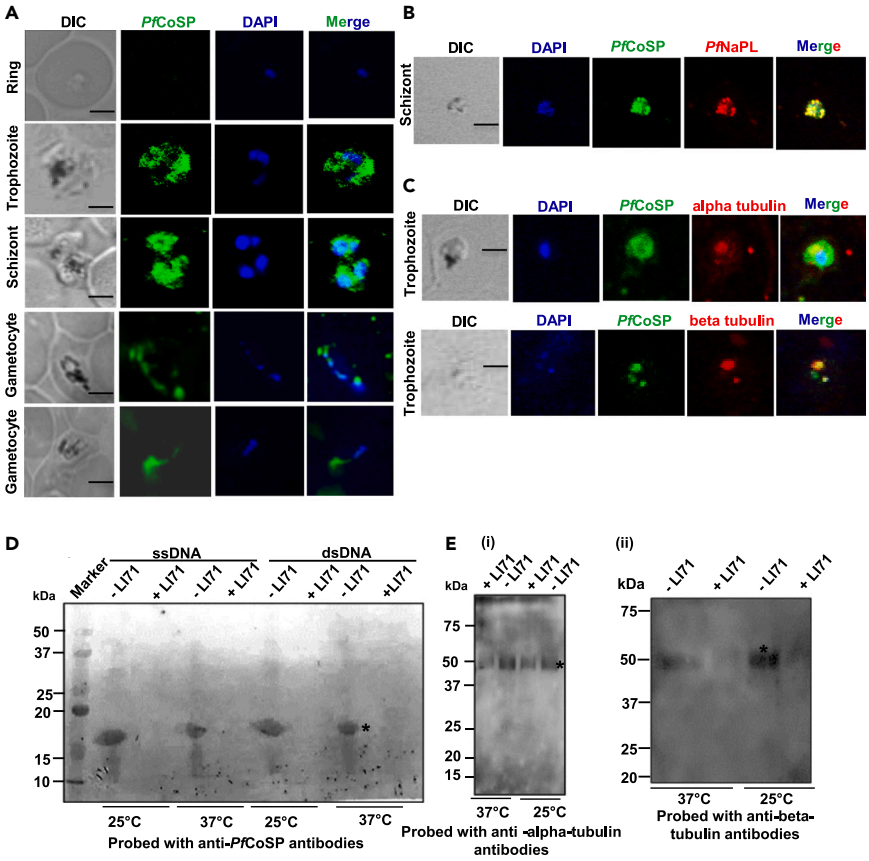

Figure 6. Expression and localization analysis of *Pf*CoSP at asexual and gametocyte stages of parasite life cycle and effect of LI71 on native *Pf*CoSP to bind with DNA and α/β tubulin

(A) Immunofluorescence images showing the localization of *Pf*CoSP at asexual and gametocyte stages of parasite life cycle. Smears of methanol-fixed *Pf*3D7-infected erythrocytes were stained with anti-*Pf*CoSP antibodies (1:250) followed by incubation with Alexa Fluor-conjugated secondary antibodies (Alexa Fluor 488, green). DIC: differential interference contrast image, DAPI: nuclear staining 40, 6-diamidino-2-phenylindole (blue); *Pf*CoSP: mouse anti-*Pf*CoSP (green); merge: overlay of *Pf*CoSP with DAPI (Scale bar: 2 μm).

(B) Co-localization of *Pf*CoSP with *Pf*NapL. Smears of methanol-fixed *Pf*3D7-infected erythrocytes were stained with anti-*Pf*CoSP (1:250) and anti-*Pf*NapL antibodies (1:250), followed by incubation with Alexa Fluor-conjugated secondary antibodies (Alexa Fluor 488, green; Alexa Fluor 594, red). DIC: differential interference contrast image, DAPI: nuclear staining 40, 6-diamidino-2-phenylindole (blue); *Pf*CoSP: mouse anti-*Pf*CoSP (green); *Pf*NapL: anti-*Pf*NapL antibody (red); merge: overlay of *Pf*CoSP with *Pf*NapL (Scale bar: 2 μm).

(C) Co-localization of *Pf*CoSP with tubulin. Smears of methanol-fixed *Pf*3D7-infected erythrocytes were stained with anti-*Pf*CoSP (1:250) and anti-tubulin antibodies (1:250), followed by incubation with Alexa Fluor-conjugated secondary antibodies (Alexa Fluor 488, green; Alexa Fluor 594, red). DIC: differential interference contrast image, DAPI: nuclear staining 40, 6-diamidino-2-phenylindole (blue); *Pf*CoSP: mouse anti-*Pf*CoSP (green); *Pf*tubulin-: anti-*Pf*tubulin antibody (red); merge: overlay of *Pf*CoSP with *Pf*tubulin (Scale bar: 2 μm).

(D) Bead based *Pf*CoSP-DNA pull down assay in the presence of LI71. Cellulose beads with immobilized single and double stranded calf thymus DNA (as mentioned on the blot) were incubated with parasite lysate treated with and without LI71 (as depicted by + and - sign on the blot) at 25°C and 37°C (mentioned below the blot). Post washing bead pellet was boiled in 1X SDS-PAGE sample loading dye followed by western blotting. Protein bands are marked with '*'.

(E) Co-immunoprecipitation assay with parasite lysate to evaluate the interaction of native *Pf*CoSP with α/β tubulin in the presence and absence of LI71. *Pf*CoSP specific antisera was coupled to aminolink plus coupling resin, and used to pull down α (i) and β tubulin (ii) from parasite culture treated with and without LI71 (as depicted by + and - sign on the blot) at 25°C and 37°C (mentioned below the blot). Elutes from the assay were probed by western blot analysis using anti-α (i) and anti-β (ii) tubulin antibodies. Protein bands are marked with '*'.

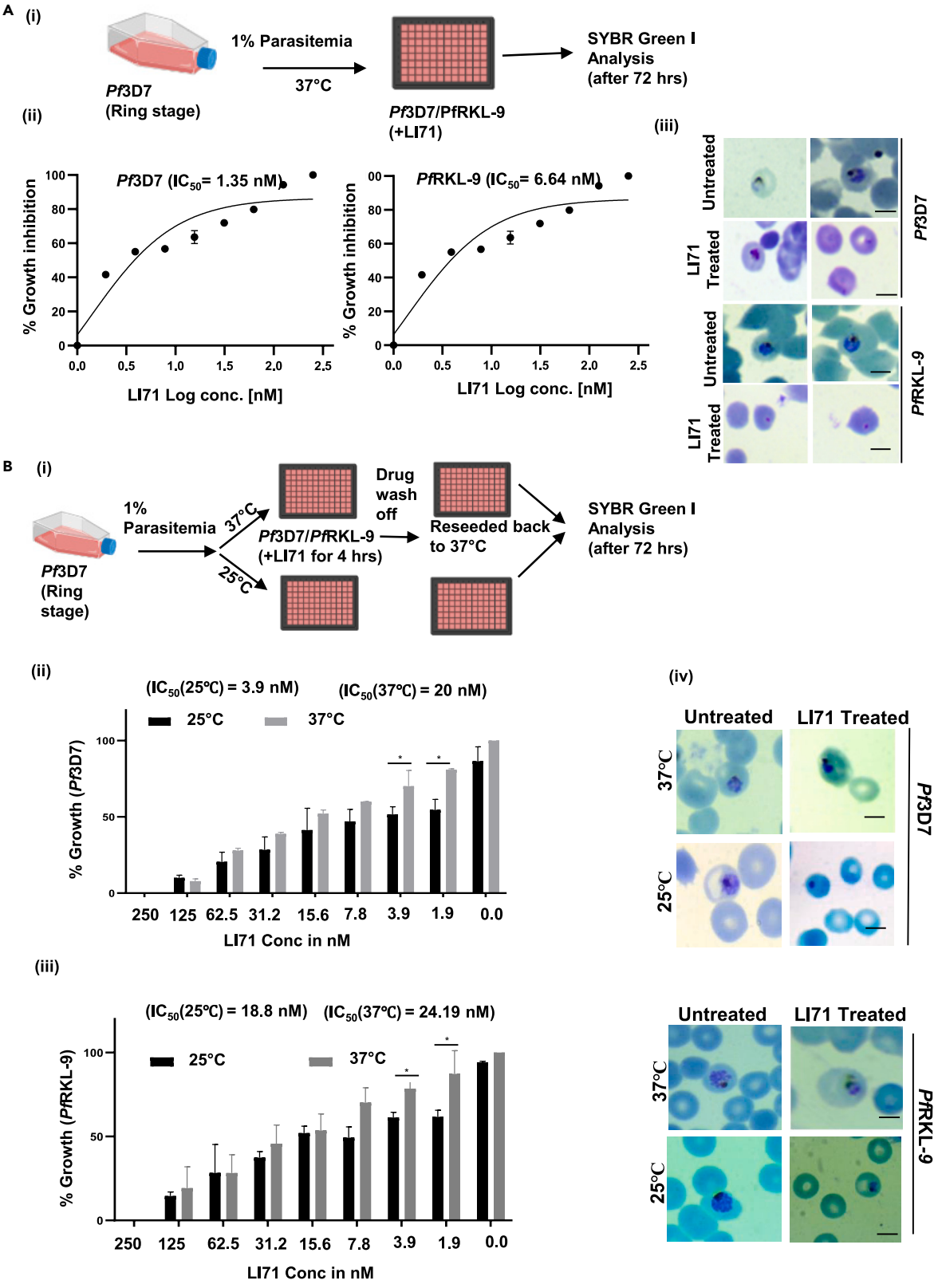
A
(i)
Pf3D7
(Ring stage)
1% Parasitemia
37°C
Pf3D7/PfRKL-9
(+LI71)
SYBR Green I
Analysis
(after 72 hrs)
(ii)
Pf3D7 (IC50= 1.35 nM)
% Growth inhibition
LI71 Log conc. [nM]
PfRKL-9 (IC50= 6.64 nM)
% Growth inhibition
LI71 Log conc. [nM]
(iii)
Untreated
LI71 Treated
Pf3D7
Untreated
LI71 Treated
PfRKL-9
B
(i)
Pf3D7
(Ring
stage)
1%
Parasitemia
37°C
25°C
Pf3D7/PfRKL-9
(+LI71 for 4 hrs)
Drug
wash
off
Reseeded back
to 37°C
SYBR Green I
Analysis
(after 72 hrs)
(ii)
(IC50(25°C) = 3.9 nM)
(IC50(37°C) = 20 nM)
25°C
37°C
% Growth (Pf3D7)
250 125 62.5 31.2 15.6 7.8 3.9 1.9 0.0
LI71 Conc in nM
(iii)
(IC50(25°C) = 18.8 nM)
(IC50(37°C) = 24.19 nM)
25°C
37°C
% Growth (PfRKL-9)
250 125 62.5 31.2 15.6 7.8 3.9 1.9 0.0
LI71 Conc in nM
(iv)
Untreated
LI71 Treated
37°C
25°C
Pf3D7
Untreated
LI71 Treated
37°C
25°C
PfRKL-9

Figure 7. Growth inhibitory effect of LI71 on *Pf*3D7 and *Pf*RKL-9

(A i) Schematic representation of methodology used in the assay. The parasite culture synchronized at ring stage was treated with different concentrations (250, 125, 62.5, 31.25, 15.62, 7.8, 3.9, 1.95 nM) of LI71 for 72 h, and the percent growth inhibition was estimated.

(A ii) IC_{50} values of LI71 in *Pf*3D7 (left panel) and *Pf*RKL-9 (right panel) were evaluated by plotting growth inhibition values against the log concentration of LI71. The experiment was done in triplicate, and the results were shown as mean values ± SD. IC_{50} values are mentioned on the plots.

(A iii) Giemsa stained images of *Pf*3D7 and *Pf*RKL-9 treated with and without LI71. (B i) Schematic representation of methodology used in cold shock *P. falciparum* growth assays. Parasite was treated with LI71 for 4 h at 25°C. After washing, culture was kept at 37°C for 68 h. As a control, parasite was treated with LI71 for 4 h at 37°C followed by a wash.

(B ii, iii) Bar diagram graph showing the growth of *Pf*3D7 (ii) and *Pf*RKL-9 strain (iii) in the presence and absence of LI71 at 25°C and 37°C. The experiment was done in triplicate, and the results were shown as mean values ± SD with p-value <0.05 *. Statistical analysis was performed using unpaired t-test. IC_{50} values at 25°C and 37°C are mentioned on the plots.

(B iv) Giemsa stained images of *Pf*3D7 and *Pf*RKL-9 treated with and without LI71 at 25°C and 37°C in cold shock *P. falciparum* growth assays.

LI71 inhibits *in vitro* growth of malaria parasites

We screened LI71 for its antiplasmodial activity against asexual stage of malaria parasite *in vitro*. Highly synchronized ring-stage parasites of *Pf*3D7 and *Pf*RKL-9 were exposed to a range of compound concentration for 72 h for IC_{50} determination. Parasitemia was measured at 72 h post-treatment using SYBR Green I based fluorescence assay and graph was plotted for the average value of three independent sets of experiments. Schematic representation of methodology used in the assay is represented in Figure 7Ai. Our results suggested potent anti-malarial activity of LI71 against 3D7 and RKL-9 strain of *P. falciparum* with a significant reduction in the parasite load. IC_{50} value of LI71 in 3D7 and RKL-9 strain of *P. falciparum* was found to be 1.35 nM and 6.3 nM respectively (Figure 7Aii). Figure 7Aiii depicts Giemsa stained images of *Pf*3D7 and *Pf*RKL-9 treated with and without LI71.

*Pf*CoSP plays a role in parasite growth during hypothermic cold stress

Our data showed that LI71 binds with *Pf*CoSP and inhibits its interaction with its binding partner tubulin. Also, LI71 showed significant anti-malarial activity. In light of above facts, we presume that LI71 inhibits the function of *Pf*CoSP *in vivo*. Because cold shock proteins play an important role in living organisms to survive under cold conditions, we hypothesize that expression of *Pf*CoSP is also required for parasite growth during temperature stress. We tested this hypothesis by inhibiting *Pf*CoSP by LI71 to know whether its inhibition influences parasite growth on cold (25°C) stress. Both *Pf*3D7 and *Pf*RKL-9 parasites were treated with inhibitor for 4 h at 25°C. Post washing, culture was kept at 37°C for 68 h. As a control, parasite was treated with LI71 for 4 h at 37°C followed by a wash. Schematic representation of methodology used in cold shock *P. falciparum* growth assays is shown in Figure 7Bi. % Growth was calculated as treated/control×100 and plotted as bar graph. Our data showed that inhibition of *Pf*CoSP by treating parasites with LI71 significantly reduced growth after temperature stress (25°C) in comparison to control (parasite treated with LI71 at 37°C) (Figures 7Bii and 7Biii). Also, the IC_{50} under temperature stress condition was found to be lower (3.968 nM in *Pf*3D7 and 19 nM in RKL-9) in comparison to control (20 nM in *Pf*3D7 and 24.41 nM in RKL-9) (Figures 7Bii and 7Biii). These data suggest that temperature stress render the parasite more susceptible to *Pf*CoSP inhibitor. Figure 7Biv depicts Giemsa stained images of *Pf*3D7 and *Pf*RKL-9 treated with and without LI71 at 25°C and 37°C. To further distinguish live verses dead parasite at 25°C and 37°C in the presence and absence of LI71 and to examine the specific effect of LI71 at low temperatures, SYTO 9 (green) and propidium iodide (PI; red)] staining was performed. SYTO 9 stains both dead and live cells whereas PI stains only dead cells. Here, *Pf*3D7 and *Pf*RKL-9 were treated with LI71 at their IC_{50} concentrations (3.968 nM for *Pf*3D7 and 19 nM for RKL-9 at 25°C and 20 nM for *Pf*3D7 and 24.41 nM for RKL-9 at 37°C) for 4 h at 25°C and 37°C. Post washing, culture was kept at 37°C for 68 h and subjected to SYTO 9 and PI staining. Fluorescence images of *Pf*3D7 (Figures 8Ai and 8Aii) and *Pf*RKL-9 ((Figures 8Aiii and 8Aiv) stained with SYTO 9 and PI post 4 h (Figures 8Ai and 8Aiii) and 72 h LI71 (Figures 8Aii and 8Aiv) treatment clearly demonstrate that the parasites are more susceptible to death because of LI71 exposure at both temperatures. Percentage of live (SYTO 9+/PI-) and dead (SYTO 9+/PI+) cells (n = 10) at 4 h and 72 h after LI71 parasite treatment at 25°C and 37°C was also plotted as bar graphs. These data further depict that parasite death is because of LI71 exposure at 25°C and 37°C (Figure 8B). Also, LI71 was effective in parasite killing post 72 h as compared to 4 h LI71 treatment (Figure 8B).

We also investigated the effect of *Pf*CoSP on growth of BL21 (DE3) *E. coli* cells transformed with its cloned plasmid by subjecting them to low temperature. Transformed cells were incubated at 20°C post protein induction for 8 h and samples were taken at 4 and 8 h of treatment. We observed that the growth of cells

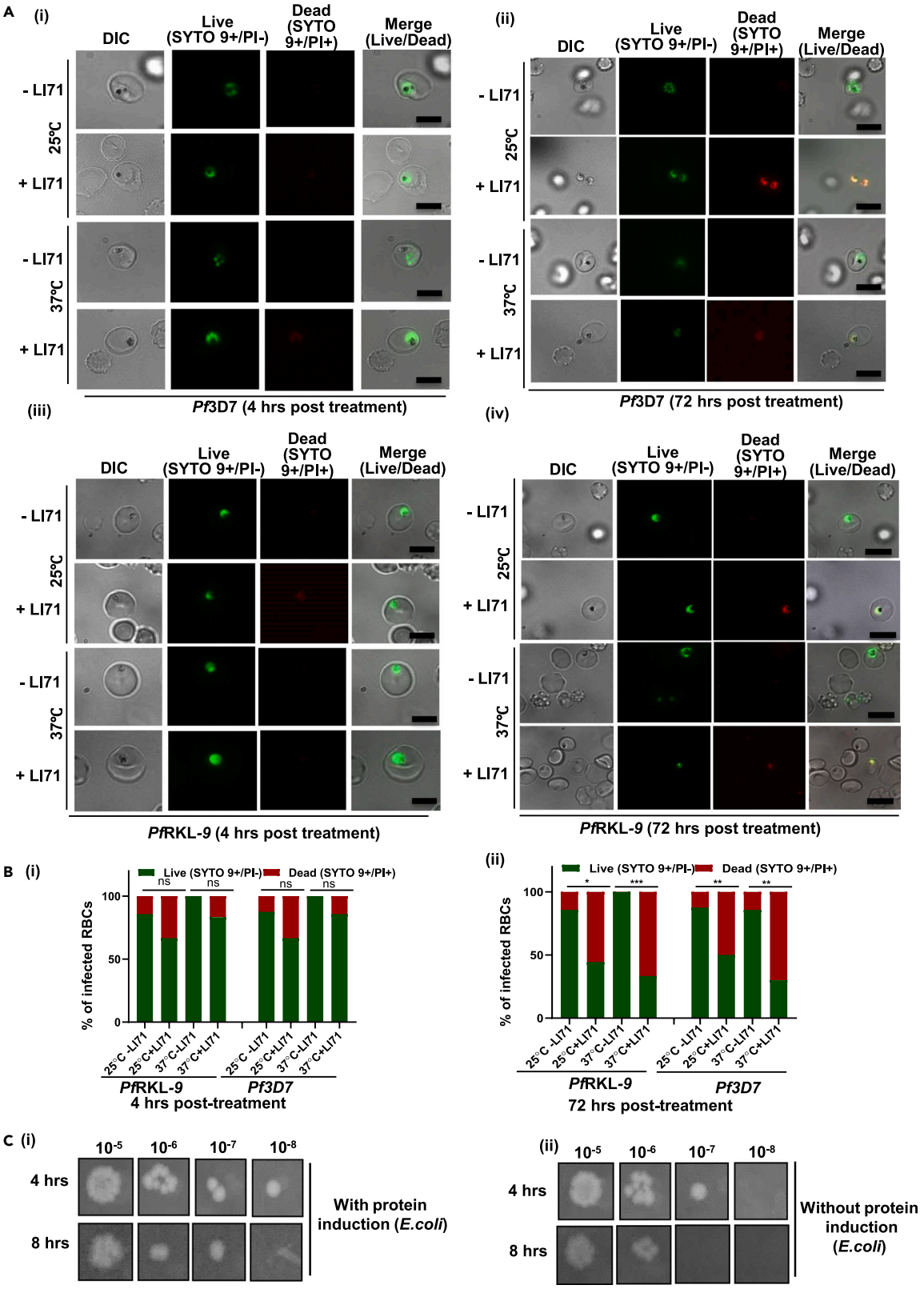
A
(i)
DIC
Live (SYTO 9+/PI-)
Dead (SYTO 9+/PI+)
Merge (Live/Dead)
- LI71
25°C
+ LI71
- LI71
37°C
+ LI71
(ii)
Pf3D7 (4 hrs post treatment)
Pf3D7 (72 hrs post treatment)
(iii)
(iv)
PfRKL-9 (4 hrs post treatment)
PfRKL-9 (72 hrs post treatment)
B
(i)
Live (SYTO 9+/PI-)
Dead (SYTO 9+/PI+)
ns
% of infected RBCs
100
50
0
25°C -LI71
25°C+LI71
37°C-LI71
37°C+LI71
PfRKL-9
Pf3D7
4 hrs post-treatment
(ii)
*
***
**
72 hrs post-treatment
C
(i)
10-5
10-6
10-7
10-8
4 hrs
8 hrs
With protein induction (E.coli)
(ii)
Without protein induction (E.coli)

Figure 8. Specific effect of LI71 on malaria parasite at 25°C and 37°C using SYTO 9 and propidium iodide (PI) staining, and growth inhibitory effect of *E. coli* BL21 cells on cold stress

(A) Fluorescence images of live (SYTO 9+/PI-) and dead (SYTO 9+/PI+) *Pf*3D7 (i, ii) and *Pf*RKL-9 (iii, iv) at 4 h (i, iii) and 72 h (ii, iv) post LI71 treatment. Here the parasite was treated with and without LI71 (denoted with +LI71 and-LI71) at 25°C and 37°C for 4 h. Post drug washing, culture was kept at 37°C for 68 h. Merge represents overlay of SYTO 9 and PI (Scale bar: 2 μm).

(B) Percentage of live (SYTO 9+/PI-) and dead (SYTO 9+/PI+) cells (n = 10) at 4 h (i) and 72 h (ii) post LI71 parasite treatment at 25°C and 37°C (mentioned below the bars). Treated parasite are represented with +LI71 and untreated with-LI71. Statistical analysis was performed using unpaired t-test and is shown with p-values <0.05 *, p-value <0.01** and 0.001***. ns represents non-significant.

(C) Growth of *E.coli* BL21 cells upon cold stress. (i) Colonies obtained after 4 h (upper panel) and 8 h (lower panel) of cold treatment in *E.coli* BL21 cells transformed with cloned plasmid of *Pf*CoSP. (ii) Control plates for comparison of growth after 4 (upper panel) and 8 h of cold treatment (lower panel) where induction was not given for *Pf*CoSP expression. Different dilutions used in the experiment are mentioned.

was more in case of transformed cells (Figure 8Ci) as compared to control where induction for *Pf*CoSP expression was not given (Figure 8Cii). This suggests that *Pf*CoSP has properties that give positive effect on growth of cells on cold stress.

LI71 effects the process of gametocytogenesis and inhibits male gamete ex-flagellation *in vitro*

LI71 was tested for its effect on gametocytogenesis in *P. falciparum* gametocyte. RKL-9 strain of *P. falciparum* was differentiated into sexual stages and treated with LI71 at 10 nM, 50 nM, 100 nM, 250 nM and 500 nM concentration. Our results suggest that daily dose of LI71 at early-stage II cause the decline in gametocytemia (Figure 9A). We also performed microscopy of blood smears and quantified gametocyte stages. Giemsa image analysis revealed that parasite treated with LI71 has altered morphology whereas gametocytes develop until stage V in DMSO treated control (Figure 9B).

We also carried out *in vitro* exflagellation assay with *P. falciparum* gametocyte to assess the effect of LI71 on male ex-flagellation. Stage V *P. falciparum* gametocyte was pre-incubated with LI71 for 1 h at concentration of 10 nM, 50 nM, 100 nM, 250 and 500 nM at 37°C. After incubation, ex-flagellation was induced by the addition of 100 μM xanthurenic acid at RT for 15 min. Afterward, the number of ex-flagellation centers were microscopically counted in both DMSO and compound treated parasites at 40× magnification. Ex-flagellation is a highly time-dependent that is defined by the emergence of the male gametes from the infected erythrocyte after a period of ~15 to 20 min. Once they emerge from the gametocyte residual body, they migrate away from the ex-flagellation center through flagellar locomotion and continue to move until they reach a female gamete and fertilize it. Since male gametes are highly motile cells, it is easy to distinguish them by light microscopy. Treatment with LI71 showed a significant reduction in the numbers of exflagellation centers by approximately 90% in comparison to DMSO control (Figure 9Ci). Light microscopic images depicting reduction in exflagellation centers of *P. falciparum* gametocytes after treatment with LI71 are represented in Figure 9Cii. These data suggest that LI71 inhibits the male gamete ex-flagellation and implicate that *Pf*CoSP may play a significant role during exflagellation.

*Pf*CoSP regulates gene expression

Cold shock proteins have been previously shown to regulate gene expression.[36] The Y-box binding protein-1 (YB-1) is a member of cold shock protein family and is known to function in humans as a positive transcription factor that upregulates several genes, including MDR1 (multi-drug resistance-1).[22] Another human cold shock protein termed, PIPPin, is known to bind to the 3′-UTR ends of histone H1 and H3.3 mRNAs and its role is indicated in the negative regulation of histone variant synthesis in the developing brain.[24] To evaluate whether *Pf*CoSP has any role in regulating gene expression, we selected some genes (*RPL7*; PF3D7_1424400, *PfAIP*; PF3D7_1136700, *H4*; PF3D7_1105000, *Pfs16*; PF3D7_0406200, *PhistB*; PF3D7_1372100, *AT2*; PF3D7_0422300, *MDV1*; PF3D7_1216500, *PfEMP1*; PF3D7_0324900, *ETRAMP10.3*; PF3D7_1016900, *ETRAMP4*; PF3D7_0423700, *CPP*; PF3D7_1146800, *H3.3*; PF3D7_0617900, *MDR1*; PF3D7_0523000, *P47*; PF3D7_1346800, *G27/25*; PF3D7_1302100, *PfEMP1-II*; PF3D7_0833500) that play a role in several critical processes of malaria parasites including chromosome organization, sexual stage development, cytoadherence, host cell invasion, drug resistance, microtubule cytoskeleton organization and translation in malaria parasite. We assessed the mRNA expression of these selected genes with *Pf*CoSP at transcript level in the presence and absence of LI71 during the asexual blood stages of *Pf*3D7. Infected erythrocytes were maintained in RPMI medium followed by treatment with *Pf*CoSP inhibitor LI71 (1.35 nM; 1x IC_{50}, 13.5 nM; 10x IC_{50} and 1 μM; 740.74x IC_{50}) and harvested after 6 h for mRNA analysis. Total RNA was extracted from the erythrocytes, and the resulting cDNA was subjected to real-time PCR, using gene-*RPL7*,

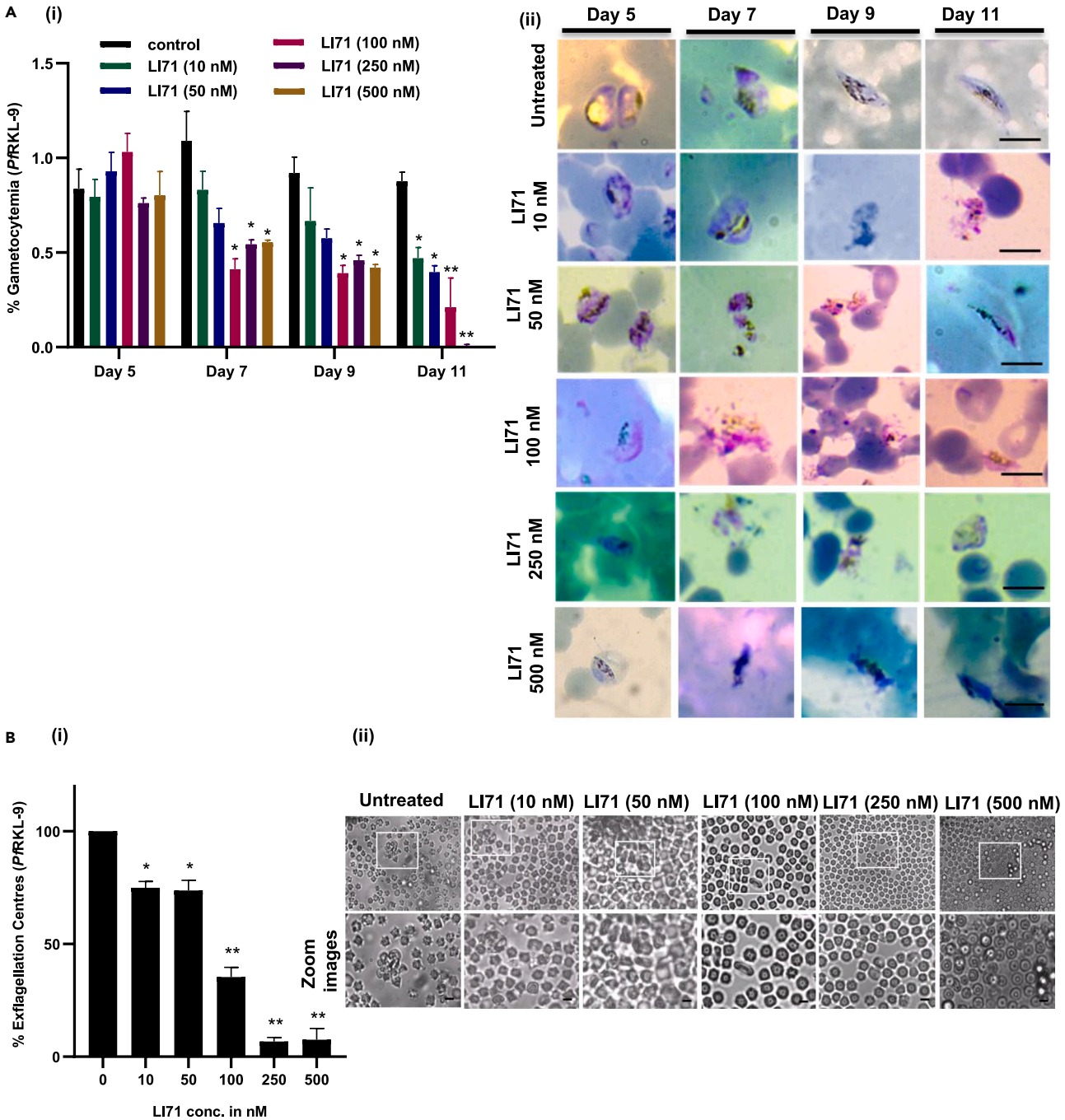

Figure 9. LI71 inhibits maturation of *Pf*-RKL9 gametocytes and ex-flagellation of male gametocytes

(A) (i) Bar graph represents number of gametocytes determined by counting Giemsa-stained smears (relative to DMSO control on day 5, 7, 9, 11) after treatment with LI71 at concentration 10, 50, 100, 250 and 500 nM. Error bars represent mean ± S.D with p-value <0.05 *, p-value <0.01**. (ii) Giemsa stained images of *Pf-RKL9* gametocytes after treatment with and without LI71 (10, 50, 100, 250 and 500 nM; Scale bar: 5 μm).

(B) LI71 inhibits ex-flagellation of male gametocyte. (i) Late stage *P. falciparum-RKL9* gametocyte was mixed with pre-warmed complete RPMI and incubated with LI71 (10, 50, 100, 250 and 500 nM) for 30 min at 37°C. Ex-flagellation was induced by transferring the sample to 25°C in the presence of 100 μM of xanthurenic for 15 min. Sample were then dispensed onto glass bottom plate and observed under bright field microscopy at 40× magnification. Bar graphs represent the no of ex-flagellation centers observed in 10 field views post addition of LI71 compound. Data represent the mean ±S.D (n = 3). Statistical analysis was calculated using unpaired t-test and is shown with p-values <0.05 * and p-value <0.01**. (ii) Light microscopic images showing reduction in exflagellation centers of *P. falciparum* gametocytes following treatment with LI71 (Scale bar: 5 μm).

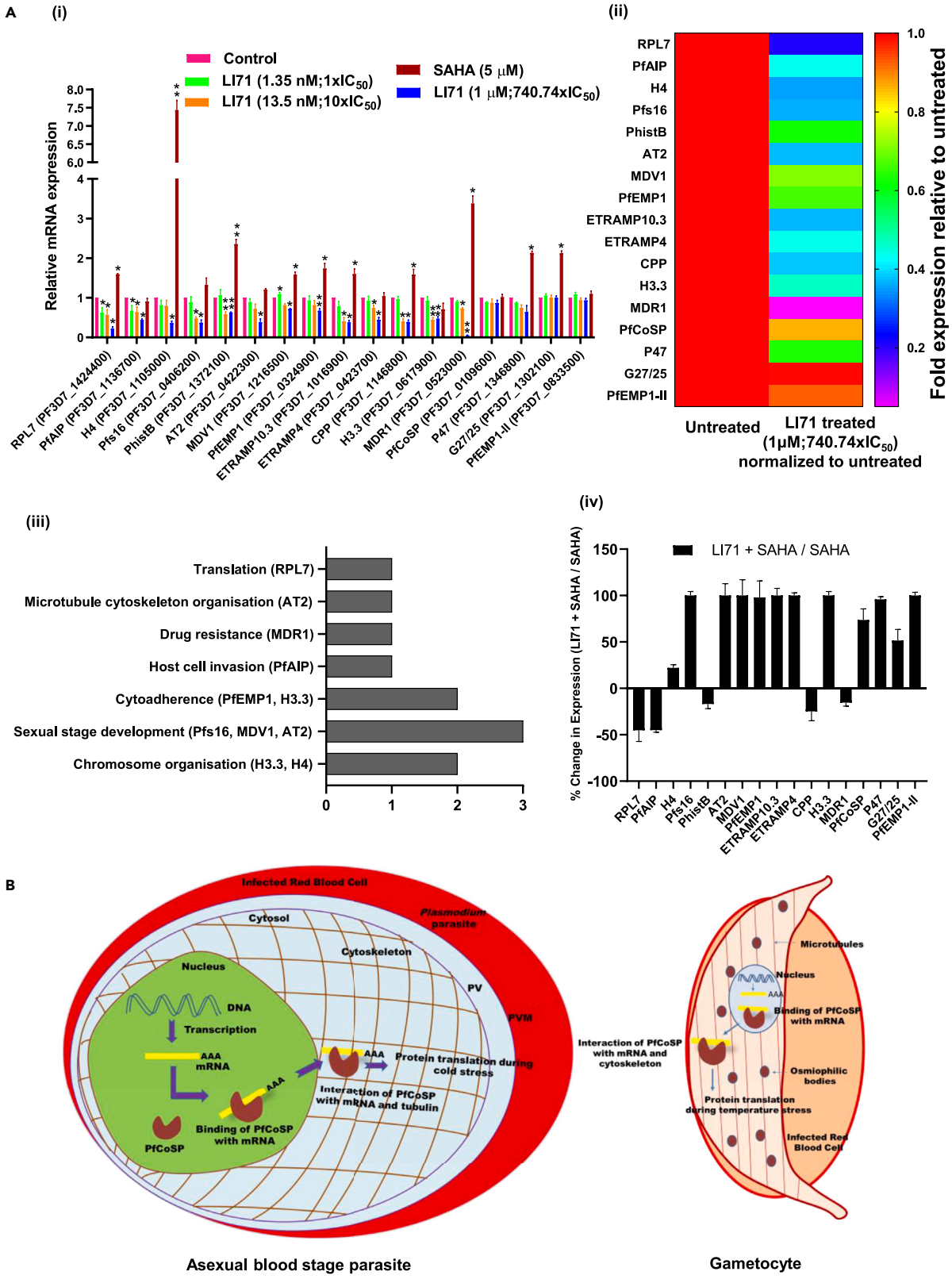
A
(i)
Control
LI71 (1.35 nM;1xIC50)
LI71 (13.5 nM;10xIC50)
SAHA (5 μM)
LI71 (1 μM;740.74xIC50)
Relative mRNA expression
RPL7 (PF3D7_1424400)
PfAIP (PF3D7_1136700)
H4 (PF3D7_1105000)
Pfs16 (PF3D7_0406200)
PhistB (PF3D7_1372100)
AT2 (PF3D7_0422300)
MDV1 (PF3D7_1216500)
PfEMP1 (PF3D7_0324900)
ETRAMP10.3 (PF3D7_1016900)
ETRAMP4 (PF3D7_0423700)
CPP (PF3D7_1146800)
H3.3 (PF3D7_0617900)
MDR1 (PF3D7_0523000)
PfCoSP (PF3D7_0109600)
P47 (PF3D7_1346800)
G27/25 (PF3D7_1302100)
PfEMP1-II (PF3D7_0833500)
(ii)
RPL7
PfAIP
H4
Pfs16
PhistB
AT2
MDV1
PfEMP1
ETRAMP10.3
ETRAMP4
CPP
H3.3
MDR1
PfCoSP
P47
G27/25
PfEMP1-II
Fold expression relative to untreated
Untreated
LI71 treated
(1μM;740.74xIC50)
normalized to untreated
(iii)
Translation (RPL7)
Microtubule cytoskeleton organisation (AT2)
Drug resistance (MDR1)
Host cell invasion (PfAIP)
Cytoadherence (PfEMP1, H3.3)
Sexual stage development (Pfs16, MDV1, AT2)
Chromosome organisation (H3.3, H4)
(iv)
LI71 + SAHA / SAHA
% Change in Expression (LI71 + SAHA / SAHA)
B
Infected Red Blood Cell
Cytosol
Plasmodium parasite
Cytoskeleton
Nucleus
PV
PVM
DNA
Transcription
AAA mRNA
Protein translation during cold stress
Interaction of PfCoSP with mRNA and tubulin
Binding of PfCoSP with mRNA
PfCoSP
Asexual blood stage parasite
Microtubules
Nucleus
Binding of PfCoSP with mRNA
Interaction of PfCoSP with mRNA and cytoskeleton
Osmiophilic bodies
Protein translation during temperature stress
Infected Red Blood Cell
Gametocyte

Figure 10. Effect of LI71 on the expression pattern of *Pf* genes and proposed model for the role of *Pf*CoSP in malaria parasite

(A i) Erythrocytes infected with *P. falciparum* were treated with LI71 (1.35 nM; 1x IC_{50}, 13.5 nM; 10x IC_{50} and 1 μM; 740.74x IC_{50}) and SAHA (5 μM) for 6 h. The total RNA was extracted, and the resulting cDNA was subjected to real-time PCR analysis using primers specific for genes mentioned below the bars. Relative fold change in expression levels were calculated using $2-\Delta\Delta Ct$ method where 18S rRNA gene was used as internal control. Values are mean ± S.D (n = 3). Statistical analysis was calculated using unpaired t-test with p-value <0.05 *, p-value <0.01**. The results are representative of three independent experiments performed in triplicates.

(A ii) Heatmap representing the relative fold change in expression levels of parasite genes after LI71 (1 μM; 740.74x IC_{50}) treatment.

(A iii) Gene ontology graph depicting the genes and their related processes (mentioned on the plot) prone to LI71-mediated transcriptional inhibition. X axis represents number of genes.

(A iv) Percentage change in expression levels of genes obtained by the combined effect of LI71 and SAHA. Erythrocytes infected with *P. falciparum* were treated with LI71 (1.35 nM; 1x IC_{50}) and SAHA (5 μM) for 6 h. Real-time PCR analysis was performed using primers specific for genes mentioned on the plot. Percentage change in expression levels were calculated as (LI71+ SAHA/SAHA)×100. Values are mean ± S.D (n = 3).

(B) Probable functional role of *Pf*CoSP at gametocyte and asexual blood stages of malaria parasite. Upon temperature stress, *Pf*CoSP may bind mRNA targets and enable their maintenance of single stranded state to pursue efficient transcription and translation. In this way, *Pf*CoSP may play a significant role in regulating gene expression at different stages of malaria parasite.

PfAIP, H4, Pfs16, PhistB, AT2, MDV1, PfEMP1, ETRAMP10.3, ETRAMP4, CPP, H3.3, P47, G27/25, PfEMP1-II, MDR1 specific primers (Figure S8). RNA derived from untreated infected erythrocytes served as a negative control. Another inhibitor 'Suberoylanilide hydroxamic acid' (SAHA) was included as a control, for the assay as it is known to inhibit the function of histone deacetylases (HDACs).[49] HDACs remove the acetyl groups from the lysine residues resulting in chromatin condensation and transcriptional repression. In the presence of SAHA, genes are transcriptionally upregulated. Our RT-PCR data showed concentration dependent effect of LI71 on transcriptional inhibition. At the highest LI71 concentration (1 μM; 740.74x IC_{50}), a profound decrease in the expression of genes [*ETRAMP4*; PF3D7_0423700 (∼65%, $p \leq 0.03$), *Pfs16;* PF3D7_0406200 (∼63%, $p \leq 0.05$), *MDV1;* PF3D7_1216500 (∼30%, $p \leq 0.02$), *PhistB;* PF3D7_1372100 (∼40%, $p \leq 0.01$), *AT2;* PF3D7_0422300 (∼30%, $p \leq 0.20$), *ETRAMP10.3;* PF3D7_1016900 (∼63%, $p \leq 0.03$), *PfEMP1;* PF3D7_0324900 (∼67%, $p \leq 0.17$), *RPL7;* PF3D7_1424400 (∼80%, $p \leq 0.04$), *AIP;* PF3D7_1136700 (∼60%, $p \leq 0.02$), *H4;* PF3D7_1105000 (∼77%, $p \leq 0.05$), *CPP;* PF3D7_1467600 (∼60%, $p \leq 0.03$), *P47*; PF3D7_1346800 (∼36%, $p \leq 0.03$)] and *H3.3*; PF3D7_0617900 (∼53%, $p \leq 0.01$), MDR1; PF3D7_0523000 (∼90%, $p \leq 0.01$)] was found (Figure 10Ai). Since LI71 treatment was given for 6 h only, its effect on transcriptional inhibition was less at its IC_{50} (1.35 nM) and 10x IC_{50} (13.5 nM) concentrations (Figure 10Ai). *P47* (PF3D7_1346800), *G27/25* (PF3D7_1302100) *and PfEMP1-II* (PF3D7_0833500) expression remain unaltered on addition of LI71 inhibitor, suggesting that LI71 does not universally significantly inhibit transcription across genes tested in the assay. Also, *Pf*CoSP expression was unaltered suggesting no effect of LI71 on the mRNA expression of protein itself. SAHA was found to upregulate the expression of genes as expected (Figure 10Ai). The heatmap in Figure 10Aii displays relative gene expression after LI71 (1 μM; 740.74x IC_{50}) treatment. Gene ontology plot depicts the genes and their related processes prone to LI71-mediated transcriptional inhibition (Figure 10Aiii). Overall, these results suggest that *Pf*CoSP may play a significant role in regulating the expression of genes that are involved in critical processes like chromosome organization, sexual stage development, cytoadherence, host cell invasion, drug resistance, microtubule cytoskeleton organization and translation.

To further assess the effect of LI71 on transcription of genes regulated by HDAC, we tested LI71 (1.35 nM; 1x IC_{50}) in combination with SAHA (5 μM). The analysis was performed to examine the effect of LI71 over SAHA, if any. Percentage change in expression levels obtained by the combined effect of LI71 and SAHA showed that LI71 has a dominant effect over SAHA in regulating the gene expression of *RPL7, AIP, PhistB, CPP, G27/25 and MDR1* (Figure 10Aiv). On the other hand, expression level of *H4, Pfs16, AT2, MDV1, PfEMP1, ETRAMP10.3, ETRAMP4, H3.3, PfCoSP, P47 and PfEMP1-II* were not significantly affected, suggesting the prominent effect of SAHA over LI71 (Figure 10Aiv).

DISCUSSION

Cold shock proteins are believed to counteract the harmful effects of low temperature by inhibiting the formation of secondary structures in mRNA, thereby facilitating the process of translation.[3,6] Members of cold shock proteins are well characterized in bacteria, plants and humans and are known for their ability to perform pleiotropic functions inside the cell.[36] In the present study, we have attempted to delineate the function of a cold shock protein (*Pf*CoSP) of malaria parasite. Knowing the *Pf* cold shock protein's molecular interactions can help us understand the biology of malaria parasite.

Full length construct of *Pf*CoSP was cloned in pET-28a(+) vector and overexpressed in soluble form in a bacterial expression system. Polyclonal antibodies were generated against *Pf*CoSP and found to be specific for the protein. Cold shock proteins are characterized by the presence of cold shock domain that exhibits nucleic acid binding properties,[3,6] therefore we tested *Pf*CoSP for DNA/RNA binding ability using *in vitro* assays. Our results clearly demonstrate that *Pf*CoSP binds with both DNA and RNA, suggesting that protein is likely to function as nucleic acid chaperone *in vivo*. Several studies have reported both DNA and RNA binding activity of cold shock proteins including YB-1 of humans, WCSP1 of wheat, AtCSP1-CSP4 of *Arabidopsis*, OsCSP1 (Os02g0121100) and OsCSP2 (Os08g0129200) of rice.[36] By nucleic acid binding ability, cold shock proteins are involved in several DNA and mRNA dependent processes including mRNA splicing and translation, DNA replication and repair, thereby regulating gene expression.[36]

It has been suggested that cytoskeleton disassembly on cold shock disrupt translational machinery which in turn inhibit protein translation at low temperatures.[37] B. al-Fageeh et al. proposed that cold shock proteins link transcription and translation via interactions with target mRNAs and the cytoskeleton.[37] In light of above facts, we examined the binding of *Pf*CoSP with components of cell cytoskeleton viz. α and β tubulin. Our *in vitro* binding assays (semi-quantitative ELISA, MST and co-immunoprecipitation assays) clearly demonstrate that recombinant *Pf*CoSP interacts with both α and β tubulin. These data suggest the potential of *Pf*CoSP to act as a cytoskeleton linking protein. Because *Pf*CoSP showed direct interaction with *Pf* tubulin, we tested the effect of *Pf*CoSP on tubulin polymerization. Our data suggests that *Pf*CoSP enhances tubulin polymerization, suggesting its role in microtubule assembly. Our previous results showed that *Pf*CoSP binds to both RNA and *Pf*tubulin, therefore we tested whether RNA and α tubulin bind with *Pf*CoSP together to form a complex, or compete with each other for attachment to *Pf*CoSP. Our results clearly depict that *Pf*CoSP binds to both RNA and α tubulin simultaneously *in vitro*. These data is suggestive of separate binding sites for RNA and α tubulin on *Pf*CoSP. This highlights the ability of *Pf*CoSP to dually function as a nucleic acid chaperone and cytoskeleton linking molecule simultaneously.

We next performed extensive literature search to identify any inhibitor for a cold shock protein. A molecule named L171 was identified that directly binds the cold shock domain of a human cold shock protein 'LIN28'.[38] By interacting with cold shock domain, LI71 suppresses activity of LIN28 against let-7 in leukemia cells and embryonic stem cells.[38] Multiple sequence alignment of *Pf*CoSP with LIN28 suggests significant similarity between the proteins. Therefore, we tested direct interaction of LI71 with *Pf*CoSP and its potential to act as an inhibitor for the protein. Our docking studies suggest that LI71 binds well into the cavity formed by cold shock domain of *Pf*CoSP. Kinetic analysis of one-to-one interaction using MST suggested significant binding of *Pf*CoSP with L171 with a K_d of 431 nM. We next tested the effect of LI71 on tubulin polymerization in the presence and absence of *Pf*CoSP and found that tubulin polymerization is inhibited in LI71 treated sample. This suggested the inhibitory effect of LI71 on *Pf*CoSP function of microtubule assembly. We went further to test LI71 for inhibiting *Pf*CoSP interaction with DNA and α/β tubulin. Our competitive inhibition assays using MST, pull down and co-immunoprecipitation assays suggested that LI71 is capable of inhibiting *Pf*CoSP-DNA and *Pf*CoSP-α/β tubulin interactions.

The study was further sought to analyze the expression and localization of *Pf*CoSP at asexual blood stages and gametocyte stage of malaria parasite. Our western blot analysis on mixed stage parasite lysates shows a single band of *Pf*CoSP at the expected size. Also, we observed that *Pf*CoSP expression upregulates when parasite was subjected to cold conditions, further highlighting its role during cold stress. Immunofluorescence data depict the expression of *Pf*CoSP during gametocyte and asexual blood stages of malaria parasite. Stage specific expression analysis suggests expression of *Pf*CoSP mainly in the trophozoite and schizont stages. Also, our immunofluorescence data depict *Pf*CoSP as a nucleo-cytoplasmic protein. Furthermore, *Pf*CoSP showed significant co-localization with *Pf* α and β tubulin suggesting the interaction between the proteins.

Our previous data provided a clue for the potential of LI71 to obstruct the functions of *Pf*CoSP and prompted us to test the antiplasmodial activity of LI71 on different stages of malaria parasite. Our growth inhibition assays clearly illustrate that LI71 inhibited the growth of blood stage *P. falciparum* 3D7 and chloroquine drug-resistant strain *Pf*RKL-9 with an IC_{50} value of 1.35 nM and 6.32 nM respectively. Also, inhibition of *Pf*CoSP with LI71 significantly reduced parasite growth post temperature stress, implicating the role of *Pf*CoSP during cold stress condition. IC_{50} of LI71 against *Pf*3D7 and *Pf*RKL-9 was found to be even lower

at cold stress. We also tested the ability of *Pf*CoSP to give any growth advantage to *E. coli* cells on cold treatment. Our results demonstrate that over-expression of *Pf*CoSP enhanced the BL21 (DE3) *E. coli* growth at hypothermic cold conditions. These data further provide hint for the functional role of *Pf*CoSP in malaria parasite when it enters the mosquito host and face low temperature. We further studied cross-stage inhibitory potential of LI71 at gametocyte stage. Our data revealed that LI71 attenuates gametocytes and inhibits the male gamete ex-flagellation *in vitro*. This complementary activity of LI71 on the sexual stages of the parasites indicates its potential to reduce malaria transmission apart from its plausible role in chemoprevention. Overall, these results illustrate antiplasmodial activity of LI71 against gametocytes and asexual blood stages of parasite.

Because cold shock proteins are known to play role in regulating gene expression, we evaluated whether *Pf*CoSP has any role in gene expression regulation by performing qRT-PCR of some crucial proteins post LI71 treatment to parasite. SAHA was also taken in the assay, which is known to inhibit the function of histone deacetylases (HDACs),[49] leading to transcriptional upregulation. Our results demonstrated that there was a significant decrease in the expression level of genes where parasite was treated with LI71. These genes downregulated by LI71 are implicated in important functions like chromosome organization, sexual stage development, cytoadherence, host cell invasion, drug resistance, microtubule cytoskeleton organization and translation. This highlights that *Pf*CoSP may play an important role in regulating the expression of genes that play critical functions in malaria parasite. We further evaluated the effect of LI71 on transcription of genes regulated by HDAC by treating parasite culture with a combination of LI71 and SAHA. Our data suggest that LI71 has a dominant effect over SAHA in regulating the gene expression of *RPL7, AIP, PhistB, CPP, G27/25 and MDR1*. This implicates that these genes are predominantly regulated by *Pf*CoSP over HDAC.

A report suggests that cytoskeleton disassembly on cold shock disrupt translational machinery and might account for the suppression of protein synthesis in mammalian cells.[37] Based on our study, we propose a model for the role of *Pf*CoSP in regulating gene expression by its nucleic acid binding ability (Figure 9B). In the model, *Pf*CoSP can capture mRNA targets as they emerge from the nucleus, or in the cytoplasm, and enable their maintenance of single stranded state to pursue efficient transcription and translation. *Pf*CoSP assists the process of translation by simultaneously interacting with mRNA targets and components of cell cytoskeleton (Figure 10B). *Pf*CoSP via interactions with the components of cell cytoskeleton also helps in forming a work bench for translation. In this way, *Pf*CoSP may play a significant role in regulating gene expression at different stages of malaria parasite.

Overall, our data highlights the potential of *Pf*CoSP in parasite growth and development on cold stress when it enters mosquito host to complete its sexual cycle. In infected humans, majority of circulating parasites are asexually dividing merozoites. A small portion of these undergo a differentiation pathway to form sexually competent parasite called 'gametocyte'. These highly specialized gametocytes are transmitted from an infected human to a susceptible mosquito host. As gametocytes switch from human host to female *Anopheles*, they egress from the host erythrocytes and face low temperature environment.[43,44] We propose that during this transitioning, *Pf*CoSP play its pivotal role in adapting the parasite to cold stress condition. Because *Pf*CoSP is essential for parasite survival, characterization of its interaction with DNA/RNA, tubulin and identification of its inhibitor 'LI71' may form the basis for development of future anti-malarials.

Limitations of the study

The study involves the use of biochemical techniques to characterize the functional roles of *Pf*CoSP in malaria parasite. The parasite response to *Pf*CoSP attenuation will help in defining and describing its involvement in parasite biology. This, however, is not feasible owing to practical limitations because *Pf*CoSP is essential for the asexual growth of parasite. It is therefore impossible to have complete genetic ablation of *Pf*CoSP. Therefore, the inherent essentiality of the gene and the practical issues with the currently known genetic modification techniques for the malaria parasite are two contributing factors to our study's limitations.

STAR★METHODS

Detailed methods are provided in the online version of this paper and include the following:

- KEY RESOURCES TABLE

SUPPLEMENTAL INFORMATION

Supplemental information can be found online at https://doi.org/10.1016/j.isci.2023.106637.

ACKNOWLEDGMENTS

AB is supported by National Post-doctoral fellowship, SERB, India (Fellowship reference no. PDF/2019/000334). RS is UGC-SRF Govt. of India, GK is CSIR-SRF Govt. of India and MS is supported by SNU-Foundation fellowship. EM and SG are CSIR SRA in scientist pool scheme and VK was supported by Research Associateship Program of Department of Biotechnology, Govt. of India. JK is DST/INSPIRE Senior research fellow. Funding from Intensification of Research in High Priority Areas (IRHPA) of Science and Engineering Research Board (SERB) and the National Bioscience Award from DBT for SS is acknowledged. This manuscript has been screened by the anti-plagiarism software turnitin. ICMR-National Institute of Malaria Research, India is acknowledged for providing RKL-9 strain of *Plasmodium falciparum*.

AUTHOR CONTRIBUTIONS

A.B.: Experimental design, experimentation, data analysis and manuscript writing. R.S.: Experimental design, experimentation, data analysis and manuscript preparation. F.D.L.: Synthesized LI71. G.K.: Conducted experiments related to antiplasmodial activity of LI71 and manuscript preparation. M.S.: Conducted assays using MST and manuscript preparation. E.M.: Conducted qRT-PCR analysis. V.K.: Experimental design, data analysis, conducted some binding assays using nanotemper and manuscript preparation. H.S.: Preparation of buffers, J.K.: Prepared graphical abstract, P.M.: Preparation of buffers, S.G.: Data analysis, P.C.M.: Preparation of PFA0660w (*Pf*Hsp40) antibodies and manuscript writing. C.A.: Syntheses of LI71, Data analysis and manuscript writing. S.S.: Conception of idea, experimental design, data analysis and manuscript writing.

DECLARATION OF INTERESTS

The authors declare no competing interests.

Received: July 15, 2022
Revised: February 16, 2023
Accepted: April 4, 2023
Published: April 11, 2023

REFERENCES

1. Ermolenko, D.N., and Makhatadze, G.I. (2002). Bacterial cold-shock proteins. Cell. Mol. Life Sci. *59*, 1902–1913. https://doi.org/10.1007/pl00012513.

2. Weber, M.H., and Marahiel, M.A. (2003). Bacterial cold shock responses. Sci. Prog. *86*, 9–75. https://doi.org/10.3184/003685003783238707.

3. Wolffe, A.P., Tafuri, S., Ranjan, M., and Familari, M. (1992). The Y-box factors: a family of nucleic acid binding proteins conserved from *Escherichia coli* to man. New Biol. *4*, 290–298.

4. Lindquist, J.A., Brandt, S., Bernhardt, A., Zhu, C., and Mertens, P.R. (2014). The role of cold shock domain proteins in inflammatory diseases. J. Mol. Med. *92*, 207–216. https://doi.org/10.1007/s00109-014-1136-3.

5. Brandt, S., Raffetseder, U., Djudjaj, S., Schreiter, A., Kadereit, B., Michele, M., Pabst, M., Zhu, C., and Mertens, P.R. (2012). Cold shock Y-box protein-1 participates in signaling circuits with auto-regulatory activities. Eur. J. Cell Biol. *91*, 464–471. https://doi.org/10.1016/j.ejcb.2011.07.002.

6. Wolffe, A.P. (1994). Structural and functional properties of the evolutionarily ancient Y-box family of nucleic acid binding proteins. Bioessays *16*, 245–251. https://doi.org/10.1002/bies.950160407.

7. Jones, P.G., and Inouye, M. (1994). The cold-shock response—a hot topic. Mol. Microbiol. *11*, 811–818. https://doi.org/10.1111/j.1365-2958.1994.tb00359.x.

8. Gottesman, S. (2018). Chilled in translation: adapting to bacterial climate change. Mol. Cell *70*, 193–194. https://doi.org/10.1016/j.molcel.2018.04.003.

9. Yamanaka, K., Fang, L., and Inouye, M. (1998). The CspA family in *Escherichia coli*: multiple gene duplication for stress adaptation. Mol. Microbiol. *27*, 247–255. https://doi.org/10.1046/j.1365-2958.1998.00683.x.

10. Jiang, W., Hou, Y., and Inouye, M. (1997). CspA, the major cold-shock protein of *Escherichia coli*, is an RNA chaperone. J. Biol. Chem. *272*, 196–202. https://doi.org/10.1074/jbc.272.1.196.

11. Lopez, M.M., Yutani, K., and Makhatadze, G.I. (1999). Interactions of the major cold shock protein of *Bacillus subtilis* CspB with single-stranded DNA templates of different base composition. J. Biol. Chem. *274*, 33601–33608. https://doi.org/10.1074/jbc.274.47.33601.

12. Lopez, M.M., and Makhatadze, G.I. (2000). Major cold shock proteins, CspA from *Escherichia coli* and CspB from *Bacillus subtilis*, interact differently with single-stranded DNA templates. Biochim. Biophys. Acta *1479*, 196–202. https://doi.org/10.1016/s0167-4838(00)00048-0.

13. Lopez, M.M., Yutani, K., and Makhatadze, G.I. (2001). Interactions of the cold shock protein CspB from *Bacillus subtilis* with single-stranded DNA. Importance of the T base content and position within the template. J. Biol. Chem. *276*, 15511–15518. https://doi.org/10.1074/jbc.M010474200.

14. Zeeb, M., and Balbach, J. (2003). Single-stranded DNA binding of the cold-shock protein CspB from *Bacillus subtilis*: NMR mapping and mutational characterization. Protein Sci. *12*, 112–123. https://doi.org/10.1110/ps.0219703.

15. Landsman, D. (1992). RNP-1, an RNA-binding motif is conserved in the DNA-binding cold shock domain. Nucleic Acids Res. *20*, 2861–2864. https://doi.org/10.1093/nar/20.11.2861.

16. Burd, C.G., and Dreyfuss, G. (1994). Conserved structures and diversity of functions of RNA-binding proteins. Science *265*, 615–621. https://doi.org/10.1126/science.8036511.

17. Theobald, D.L., Mitton-Fry, R.M., and Wuttke, D.S. (2003). Nucleic acid recognition by OB-fold proteins. Annu. Rev. Biophys. Biomol. Struct. *32*, 115–133. https://doi.org/10.1146/annurev.biophys.32.110601.142506.

18. Lindquist, J.A., and Mertens, P.R. (2018). Cold shock proteins: from cellular mechanisms to pathophysiology and disease. Cell Commun. Signal. *16*, 63. https://doi.org/10.1186/s12964-018-0274-6.

19. Chen, C.Y., Gherzi, R., Andersen, J.S., Gaietta, G., Jürchott, K., Royer, H.D., Mann, M., and Karin, M. (2000). Nucleolin and YB-1 are required for JNK-mediated interleukin-2 mRNA stabilization during T-cell activation. Gene Dev. *14*, 1236–1248.

20. Capowski, E.E., Esnault, S., Bhattacharya, S., and Malter, J.S. (2001). Y box-binding factor promotes eosinophil survival by stabilizing granulocyte-macrophage colony-stimulating factor mRNA. J. Immunol. *167*, 5970–5976. https://doi.org/10.4049/jimmunol.167.10.5970.

21. Gaudreault, I., Guay, D., and Lebel, M. (2004). YB-1 promotes strand separation *in vitro* of duplex DNA containing either mispaired bases or cisplatin modifications, exhibits endonucleolytic activities and binds several DNA repair proteins. Nucleic Acids Res. *32*, 316–327. https://doi.org/10.1093/nar/gkh170.

22. Chattopadhyay, R., Das, S., Maiti, A.K., Boldogh, I., Xie, J., Hazra, T.K., Kohno, K., Mitra, S., and Bhakat, K.K. (2008). Regulatory role of human AP-endonuclease (APE1/Ref-1) in YB-1-mediated activation of the multidrug resistance gene MDR1. Mol. Cell Biol. *28*, 7066–7080. https://doi.org/10.1128/MCB.00244-08.

23. Pfeiffer, J.R., McAvoy, B.L., Fecteau, R.E., Deleault, K.M., and Brooks, S.A. (2011). CARHSP1 is required for effective tumor necrosis factor alpha mRNA stabilization and localizes to processing bodies and exosomes. Mol. Cell Biol. *31*, 277–286. https://doi.org/10.1128/MCB.00775-10.

24. Nastasi, T., Scaturro, M., Bellafiore, M., Raimondi, L., Beccari, S., Cestelli, A., and di Liegro, I. (1999). PIPPin is a brain-specific protein that contains a cold-shock domain and binds specifically to H1 and H3. 3 mRNAs. J. Biol. Chem. *274*, 24087–24093. https://doi.org/10.1074/jbc.274.34.24087.

25. Guo, A.X., Cui, J.J., Wang, L.Y., and Yin, J.Y. (2020). The role of CSDE1 in translational reprogramming and human diseases. Cell Commun. Signal. *18*, 14. https://doi.org/10.1186/s12964-019-0496-2.

26. Jin, J., Jing, W., Lei, X.X., Feng, C., Peng, S., Boris-Lawrie, K., and Huang, Y. (2011). Evidence that Lin28 stimulates translation by recruiting RNA helicase A to polysomes. Nucleic Acids Res. *39*, 3724–3734. https://doi.org/10.1093/nar/gkq1350.

27. Sasaki, K., and Imai, R. (2011). Pleiotropic roles of cold shock domain proteins in plants. Front. Plant Sci. *2*, 116. https://doi.org/10.3389/fpls.2011.00116.

28. Radkova, M., Vítámvás, P., Sasaki, K., and Imai, R. (2014). Development-and cold-regulated accumulation of cold shock domain proteins in wheat. Plant Physiol. Biochem. *77*, 44–48. https://doi.org/10.1016/j.plaphy.2014.01.004.

29. Kim, M.H., Sasaki, K., and Imai, R. (2009). Cold shock domain protein 3 regulates freezing tolerance in Arabidopsis thaliana. J. Biol. Chem. *284*, 23454–23460. https://doi.org/10.1074/jbc.M109.025791.

30. Park, S.J., Kwak, K.J., Oh, T.R., Kim, Y.O., and Kang, H. (2009). Cold shock domain proteins affect seed germination and growth of Arabidopsis thaliana under abiotic stress conditions. Plant Cell Physiol. *50*, 869–878. https://doi.org/10.1093/pcp/pcp037.

31. Fusaro, A.F., Bocca, S.N., Ramos, R.L.B., Barrôco, R.M., Magioli, C., Jorge, V.C., Coutinho, T.C., Rangel-Lima, C.M., De Rycke, R., Inzé, D., et al. (2007). AtGRP2, a cold-induced nucleo-cytoplasmic RNA-binding protein, has a role in flower and seed

development. Planta *225*, 1339–1351. https://doi.org/10.1007/s00425-006-0444-4.

32. Chaikam, V., and Karlson, D. (2008). Functional characterization of two cold shock domain proteins from *Oryza sativa*. Plant Cell Environ. *31*, 995–1006. https://doi.org/10.1111/j.1365-3040.2008.01811.x.

33. Aurrecoechea, C., Brestelli, J., Brunk, B.P., Dommer, J., Fischer, S., Gajria, B., Gao, X., Gingle, A., Grant, G., Harb, O.S., et al. (2009). PlasmoDB: a functional genomic database for malaria parasites. Nucleic Acids Res. *37*, D539–D543. https://doi.org/10.1093/nar/gkn814.

34. Sanderson, T., and Rayner, J.C. (2017). PhenoPlasm: a database of disruption phenotypes for malaria parasite genes. Wellcome Open Res. *2*, 45. https://doi.org/10.12688/wellcomeopenres.11896.2.

35. Zhang, M., Wang, C., Otto, T.D., Oberstaller, J., Liao, X., Adapa, S.R., Udenze, K., Bronner, I.F., Casandra, D., Mayho, M., et al. (2018). Uncovering the essential genes of the human malaria parasite Plasmodium falciparum by saturation mutagenesis. Science *360*, eaap7847. https://doi.org/10.1126/science.aap7847.

36. Behl, A., Kumar, V., Shevtsov, M., and Singh, S. (2020). Pleiotropic roles of cold shock proteins with special emphasis on unexplored cold shock protein member of Plasmodium falciparum. Malar. J. *19*, 382. https://doi.org/10.1186/s12936-020-03448-6.

37. Al-Fageeh, M.B., and Smales, C.M. (2006). Control and regulation of the cellular responses to cold shock: the responses in yeast and mammalian systems. Biochem. J. *397*, 247–259. https://doi.org/10.1042/BJ20060166.

38. Wang, L., Rowe, R.G., Jaimes, A., Yu, C., Nam, Y., Pearson, D.S., Zhang, J., Xie, X., Marion, W., Heffron, G.J., et al. (2018). Small-molecule inhibitors disrupt let-7 oligouridylation and release the selective blockade of let-7 processing by LIN28. Cell Rep. *23*, 3091–3101. https://doi.org/10.1016/j.celrep.2018.04.116.

39. Schneidman-Duhovny, D., Inbar, Y., Nussinov, R., and Wolfson, H.J. (2005). PatchDock and SymmDock: servers for rigid and symmetric docking. Nucleic Acids Res. *33*, W363–W367. https://doi.org/10.1093/nar/gki481.

40. Jendele, L., Krivak, R., Skoda, P., Novotny, M., and Hoksza, D. (2019). PrankWeb: a web server for ligand binding site prediction and visualization. Nucleic Acids Res. *47*, W345–W349. https://doi.org/10.1093/nar/gkz424.

41. Jerabek-Willemsen, M., Wienken, C.J., Braun, D., Baaske, P., and Duhr, S. (2011). Molecular interaction studies using microscale thermophoresis. Assay Drug Dev. Technol. *9*, 342–353. https://doi.org/10.1089/adt.2011.0380.

42. Lahondère, C., and Lazzari, C.R. (2013). Thermal stress and thermoregulation during feeding in mosquitoes Anopheles mosquitoes-New insights into malaria vectors. IntechOpen. https://doi.org/10.5772/56288.

43. Ngwa, C.J., Rosa, T.F., and Pradel, G. (2016). The Biology of Malaria Gametocytes (Rijeka, Croatia: IntechOpen). https://doi.org/10.5772/65464.

44. Ogwan'g, R.A., Mwangi, J.K., Githure, J., Were, J.B., Roberts, C.R., and Martin, S.K. (1993). Factors affecting exflagellation of *in vitro*-cultivated *Plasmodium falciparum* gametocytes. Am. J. Trop. Med. Hyg. *49*, 25–29. https://doi.org/10.4269/ajtmh.1993.49.25.

45. Delves, M.J., Straschil, U., Ruecker, A., Miguel-Blanco, C., Marques, S., Dufour, A.C., Baum, J., and Sinden, R.E. (2016). Routine in vitro culture of *P. falciparum* gametocytes to evaluate novel transmission-blocking interventions. Nat. Protoc. *11*, 1668–1680. https://doi.org/10.1038/nprot.2016.096.

46. Billker, O., Shaw, M.K., Margos, G., and Sinden, R.E. (1997). The roles of temperature, pH and mosquito factors as triggers of male and female gametogenesis of *Plasmodium berghei in vitro*. Parasitology *115*, 1–7. https://doi.org/10.1017/s0031182097008895.

47. Bennink, S., Kiesow, M.J., and Pradel, G. (2016). The development of malaria parasites in the mosquito midgut. Cell Microbiol. *18*, 905–918. https://doi.org/10.1111/cmi.12604.

48. Kuehn, A., and Pradel, G. (2010). The coming-out of malaria gametocytes. J. Biomed. Biotechnol. *2010*, 976827. https://doi.org/10.1155/2010/976827.

49. Andrews, K.T., Gupta, A.P., Tran, T.N., Fairlie, D.P., Gobert, G.N., and Bozdech, Z. (2012). Comparative gene expression profiling of P. falciparum malaria parasites exposed to three different histone deacetylase inhibitors. PLoS One *7*, e31847. https://doi.org/10.1371/journal.pone.0031847.

50. Leenaars, M., and Hendriksen, C.F.M. (2005). Critical steps in the production of polyclonal and monoclonal antibodies: evaluation and recommendations. ILAR J. *46*, 269–279. https://doi.org/10.1093/ilar.46.3.269.

51. Kumari, G., Jain, R., Kumar Sah, R., Kalia, I., Vashistha, M., Singh, P., Prasad Singh, A., Samby, K., Burrows, J., and Singh, S. (2022). Multistage and transmission-blocking tubulin targeting potent antimalarial discovered from the open access MMV Pathogen Box. Biochem. Pharmacol. *203*, 115154. https://doi.org/10.1016/j.bcp.2022.115154.

52. Trager, W., and Jensen, J.B. (1976). Human malaria parasites in continuous culture. Science *193*, 673–675. https://doi.org/10.1126/science.781840.

STAR★METHODS

KEY RESOURCES TABLE

REAGENT or RESOURCE	SOURCE	IDENTIFIER
Antibodies		
Goat anti-Mouse IgG (H + L) Cross-Adsorbed Secondary Antibody, Alexa Fluor™ 488	Invitrogen™	Cat # A-11001;RRID: AB_2534069
Goat anti-Rabbit IgG (H + L) Cross-Adsorbed Secondary Antibody, Alexa Fluor™ 594	Invitrogen™	Cat # A-11012;RRID: AB_141359
Chemicals, peptides, and recombinant proteins		
RPMI Medium 1640	Gibco™	Cat # 23400013
Hypoxanthin	Sigma-Aldrich	Cat #H9377
AlbumaxII	Gibco	Cat # 11021037
Fetal Bovine Serum	Gibco	Cat # 10270-106
Freund's Complete Adjuvants	Sigma-Aldrich	Cat #F5881
Freund's incomplete Adjuvants	Sigma-Aldrich	Cat #F5506
Deoxyribonucleic acid-cellulose double-stranded from calf Thymus DNA	Sigma-Aldrich	Cat #D8515
Deoxyribonucleic acid-cellulose single-stranded from calf Thymus DNA	Sigma-Aldrich	Cat #D8273
PowerUp™ SYBR™ Green Master Mix	Applied Biosystems™	Cat # A25742
3,3-Diaminobenzidin	Sigma-Aldrich	Cat #D8001
N-Acetyl-D-glucosamine	Sigma-Aldrich	Cat # A3286
ProLong™ Gold Antifade Mountant with DAPI	Invitrogen™	Cat #P36935
TRIzol™ Reagent	Invitrogen™	Cat # 15596026
Critical commercial assays		
Pierce™ Co-Immunoprecipitation Kit	Thermo Scientific™	Cat # 26149
High-Capacity cDNA Reverse Transcription Kit	Applied Biosystems™	Cat # 4368814
Monolith Protein Labeling Kit RED-NHS 2ND Generation (Amine Reactive)	nanoTEMPER	Cat # MO-L011
Experimental models: Organisms/strains		
Plasmodium falciparum 3D7 strain	Malaria Research and Reference Reagent Resource Center (MR4)	NA
Plasmodium falciparum RKL-9 strain	ICMR-National Institute of Malaria Research, India	NA
Software and algorithms		
ImageJ	NIH	https://imagej.nih.gov/ij
Graphpad Prism	GraphPad Prism Software	https://www.graphpad.com/scientific-software/prism/
Biorender	NA	https://www.biorender.com/

RESOURCE AVAILABILITY

Lead contact

Further information and requests for resources and reagents should be directed to and will be fulfilled by the lead contact, Prof. Shailja Singh (shailja.jnu@gmail.com).

Materials availability

This study did not generate new unique reagents.

Data and code availability

- The published article and supplemental information include all data generated and analyzed during this study.
- This paper does not report original code.
- Any additional information supporting the current study in this paper is available from the lead contact upon request.

EXPERIMENTAL MODEL AND SUBJECT DETAILS

Parasite culture

P. falciparum 3D7 parasites were cultured in O+ RBCs using complete RPMI 1640 medium (Gibco, USA) supplemented with 0.5 g/L Albumax I (Gibco, USA), 27.2 mg/L hypoxanthine (Sigma, USA) and 2 g/L sodium bicarbonate (Sigma, USA). Culture was maintained at 37°C in 90% N_2, 5% CO_2, and 5% O_2 containing environment and maintained at 5% haematocrit and 5% parasitaemia. Cultures were harvested by centrifugation from *Plasmodium* cultures (Parasitemia 8–10%) and the parasites were released from red blood cells by treatment with 0.15% saponin. Parasite pellet was washed with 1X PBS and stored at −80°C for experiments. RNA was isolated from infected RBCs using TRIzol reagent. DNA was removed by the DNase treatment kit (DNA-free DNA Removal Kit, Invitrogen, Thermo Fisher Scientific, Massachusetts, USA). Parasites were synchronized by 5% sorbitol (Sigma) selection of rings and late trophozoites or schizonts were purified from mixed parasite culture using 65% Percoll (Sigma).

METHOD DETAILS

Molecular cloning, over-expression and purification of *Pf*CoSP

Full-length gene of PF3D7_0109600 (*Pf*CoSP) was amplified by PCR using specific primers and *P. falciparum*-cDNA as template before cloning into bacterial expression vector pET28a+. After screening the transformed *E. coli* DH5α cells for positive clones by restriction digestion, recombinant vector carrying sequence for *Pf*CoSP was transformed in BL21 (DE3) *E. coli* cells. Expression of *Pf*CoSP was induced with 1 mM IPTG at 37°C for 4 h. Purification of recombinant protein was achieved by affinity chromatography.

Raising polyclonal antisera against *Pf*CoSP

Purified recombinant protein was used as immunogens to raise polyclonal antibodies in house against *Pf*CoSP in male BALB/c mice following standard protocol.[50] Mice were immunized using an emulsion that included a 1:1 ratio of Freund's complete adjuvant and antigen. Post this, animals were given three booster injections at an interval of 14 days and final bleed was then collected. Booster doses contain 1:1 ratio of freund's incomplete adjuvant and antigen.

Bead based *Pf*CoSP-DNA pull down assay

The nucleic acid binding property of protein was evaluated using cellulose beads with immobilized single and double stranded calf thymus DNA (Sigma Aldrich, USA). Here, 1 μg of recombinant *Pf*CoSP was mixed with 500 μL cellulose matrix (1 mg/mL) and incubated at 4°C for 30 min. 200 μL buffer was used to wash bead pellet. Post washing, beads were boiled in 1X SDS-PAGE sample loading dye and loaded on 15% SDS-PAGE.

Cellulose beads with immobilized single and double stranded calf thymus DNA were also used to test whether LI71 can inhibit *Pf*CoSP interaction with DNA/RNA. Here 500 μL cellulose matrix (1 mg/mL) was incubated with mixed stage parasite lysate treated with and without LI71 (1 μM) at 25°C and 37°C for 6 h. 200 μL buffer was used to wash bead pellet. Post washing, beads were boiled in 1X SDS-PAGE sample loading dye and loaded on 15% SDS-PAGE. Samples were subjected to western blotting and probed with anti-*Pf*CoSP antibodies.

Gel retardation assay

DNA/RNA binding property of protein was determined by gel retardation assay. Purified recombinant protein (1 μg) was incubated with 100 ng *Pf*DNA and *Pf*RNA in 2X nucleic acid binding buffer (3 mM $MgCl_2$, 50%

glycerol, 1M HEPES, 100 mM DTT, 1M tris-Cl pH 8) at 37ºC for 1 h. Migration patterns of nucleic acid samples incubated with protein was studied by agarose gels stained with ethidium bromide.

Binding and inhibition assays using Microscale Thermophoresis (MST)

The kinetic measurements of *Pf*CoSP-gDNA/RNA binding were conducted using Monolith NT.115 instrument (NanoTemper Technologies, Munich, Germany). 10 μM *Pf*CoSP was labeled using 30 μM Lysine reactive dye (Monolith Series Protein Labeling Kit RED-NHS second Generation) and incubated for 30 min. The labeled protein was passed through an equilibrated column (provided in the kit) and elution fractions were collected followed by subjecting the elutions to fluorescence count. The concentration of labeled *Pf*CoSP protein was kept constant at a concentration of 90 nM. The unlabeled binding partners, gDNA (2 pM) and RNA (100 nM) of *P. falciparum* were serially diluted in decreasing concentrations and titrated against constant concentration of the labeled *Pf*CoSP in 1:1 dilution. Samples were diluted in 1x PBS/0.01% Tween 20 buffer. Samples were incubated for 15 min at room temperature, followed by centrifugation at 8000 rpm for 10 min at room temperature. The samples were taken into the capillaries (K002 Monolith NT.115) and thermophoretic mobility was analyzed. Data evaluation was performed with the Monolith software (Nano Temper, Munich, Germany).

We also evaluated interaction of alpha and beta tubulin with *Pf*CoSP using Monolith NT.115 instrument. 20 μM each of alpha and beta tubulin recombinant proteins in 1X PBS buffer, pH 7.5, were fluorescently labeled per the instruction mentioned above. Simultaneously, 30 μM recombinant *Pf*CoSP was serially diluted with decreasing concentrations in 1X PBS/0.01% Tween-20 and was titrated against constant concentration of the labeled alpha and beta tubulin proteins and were analyzed as mentioned above.

Similar protocol was followed to investigate the interaction of *Pf*CoSP with LI71. 10 μM *Pf*CoSP was labeled and the concentration of labeled *Pf*CoSP was kept constant at a concentration of 626 nM. The unlabeled binding partner LI71 was serially diluted with maximum concentration at 20 μM and titrated in 1:1 dilution against labeled *Pf*CoSP.

To assess the competitive property of LI71 to interfere the interaction between gDNA and *Pf*CoSP, we performed affinity-based interaction analyses using Thiazole Orange (TO). 0.676 pM *P. falciparum* gDNA was labeled with 30 pM TO in dark followed by titration against serially diluted 10-fold in 1X PBS/0.01% Tween-20 *Pf*CoSP at the highest concentration of 150 μM in equal volumes. The samples were incubated for 15 min, thereafter, MST signals were measured. Competitive properties of compound LI71 to interfere *Pf*CoSP-gDNA interaction was studied. TO labeled gDNA was mixed with *Pf*CoSP at room temperature and incubated for 15 min followed by titration against serially diluted LI71 starting at maximal concentration of 20 μM. The samples were processed further as mentioned above.

We further performed competition experiments using MST to analyze affinity-based interaction of ligand molecules alpha and beta tubulin competing with LI71 to interact with *Pf*CoSP. To serve this purpose, labeled alpha and beta tubulin were mixed with 10 μM *Pf*CoSP at room temperature and incubated for 15 min. To this stock solution, serially diluted compound LI71 starting at 20 μM was added in equal amount. The samples were processed further as mentioned above.

Plate based interaction studies

In vitro interactions of *Pf*CoSP with alpha and beta tubulin were investigated by indirect ELISA. 100 ng each of purified alpha and beta tubulin were coated on ELISA plates and blocked with 5% BSA in PBS overnight at 4°C. The coated ligands were incubated with increasing concentrations of *Pf*CoSP (range: 10 ng–500 ng) for 2 h at room temperature, followed by extensive washing with 1X PBS. Washed plates were incubated with anti- *Pf*CoSP (1:5000) followed by anti-mice HRP conjugated secondary antibodies (1:10,000) for 2 h. Plates were developed using 1 mg/mL OPD (*o*-phenylenediamine dihydrochloride) containing H_2O_2, and absorbance measured at 490 nm.

Co-immunoprecipitation assay

Pierce chemical co-immunoprecipitation kit was used according to the manufacturer's protocol to evaluate native interaction of *Pf*CoSP and alpha and beta tubulin. Briefly, 10 μL of coupling resin was cross-linked with anti-*Pf*CoSP and anti-alpha/beta tubulin antibodies for 2 h. After extensive washing, antibody coupled resin was incubated with parasite lysate. Unbound proteins were removed by repeated washing with

binding buffer, followed by elution of prey proteins. As a negative control, preimmune sera were coupled to the resin before incubation with parasite lysate. Samples of bound proteins were resolved on 12% SDS-PAGE and subjected to western blot analysis using anti-*Pf*CoSP and anti-alpha/beta tubulin antibodies.

Similar protocol was followed to test the effect of LI71 on *Pf*CoSP interaction with alpha and beta tubulin. Here *Pf*CoSP specific antisera was coupled to aminolink plus coupling resin, and used to pull down alpha and beta tubulin from parasite culture treated with and without LI71 (1 μM) at 37°C and 25°C for 6 h. Elutes from the assay were probed by western blot analysis using anti-alpha/beta tubulin antibodies.

In vitro polymerisation assay

Pf-tubulin polymerization was carried out in 100 μL of a ice-cold re-assembly buffer (100 mM PIPES, pH 6.9, 10% glycerol, 2 mM $MgCl_2$.H2O, 0.5 mM EGTA), containing 1 mM GTP, and *Pf* alpha and *Pf* β-tubulins at 10 μM concentration.[51] The reaction mixture was prepared in clear, flat bottom 96 wells plates. The time-course of tubulin polymerization was followed over 30 min at 37°C by monitoring a change in turbidity at 350 nm using a Varioskan LUX multimode microplate reader (Thermo Scientific) equipped with an incubator for temperature control. To test whether *Pf*CoSP can accelerate the microtubule assembly, tubulin polymerisation experiments were carried out in presence of *Pf*CoSP (10 μM). Further to see the effect of LI71 on tubulin polymerization, 100 μL of the tubulin reaction mixture (containing 10 μM of *Pf* alpha, *Pf* beta-tubulins and *Pf*CoSP), was added to the 96-wells plate along with 1 μM of LI71, and the time-course of tubulin polymerization was followed over 30 min.

Complex binding assay

In-vitro formation of a complex between *Pf*CoSP, RNA/DNA and alpha/beta tubulin were tested using cellulose beads with immobilized single and double stranded calf thymus DNA (Sigma Aldrich, USA). 1 μg of *Pf*CoSP was mixed with 500 μL cellulose matrix (1 mg/mL) and incubated at 4°C for 30 min. Bead pellet was extensively washed with 200 μL buffer followed by incubation with 5 μg recombinant purified alpha/beta tubulin. After washing, beads were boiled in 1X SDS-PAGE sample loading dye before loading on 12% SDS-PAGE. Immunoblotting was performed to probe for *Pf*CoSP and alpha/beta tubulin using anti- *Pf*CoSP and anti-alpha/beta tubulin antibodies respectively on the same blot. *Pf*CoSP was incubated with cellulose beads with immobilized single and double stranded calf thymus DNA separately as positive controls. BSA was incubated with beads separately and incubated with alpha/beta tubulin as negative controls.

Real-time PCR

Expression of *Pf*CoSP was evaluated at transcript level in asexual blood stages of *Pf*3D7 by real-time PCR (StepOnePlus Real time PCR system Applied Biosystems, USA). The 18S rRNA gene of *P. falciparum* was chosen as a positive control. 10-μL reaction mixture comprises 1 μL of cDNA (1 μg), 5 μL of SYBR Green PCR Master Mix (Applied Biosystems) and 1 μL (5 mM) of *Pf*CoSP specific forward and reverse primer. The PCR conditions consisted of an initial denaturation at 95°C for 5 min, followed by amplification for 40 cycles of 15 s at 95°C, 5 s at 55°C, and 1 min at 72°C, with fluorescence acquisition at the end of each extension step. Amplification was immediately followed by a melt program consisting of 15 s at 95°C, 1 min at 60°C, and a stepwise temperature increase of 0.3 °C/s until 95°C, with fluorescence acquisition at each temperature transition.

In vitro expression analysis of *Pf*CoSP

For *Pf*CoSP expression analysis, *Pf*3D7 mixed stage asexual cultures (parasitemia ~8%) were subjected to saponin lysis (0.15% w/v) followed by extensive washing of parasite pellet with 1x PBS to remove traces of hemoglobin. Protein extract of infected and uninfected RBCs (negative control) were resolved on SDS-PAGE and transfer to NC membrane followed by blocking in 5% BSA for overnight at 4°C. Following blocking, the membrane was washed with PBS (Phosphate buffer saline) followed by probing with specific antisera against *Pf*CoSP (1:4000) for 2 h. Post washing with PBST (0.025%) and PBS, NC membrane was hybridized with horseradish peroxidise (HRP)-conjugated secondary antibodies for 2 h. Membrane was subsequently washed with PBST (0.025%) and PBS, and developed with DAB/H_2O_2 substrate.

Cold shock assay in *P. falciparum*

Synchronised schizont-stage cultures at 4% haematocrit and 8% parasitaemia were exposed to temperatures at 25°C, 37°C and 42°C for 6 h. Parasite pellet was boiled in 1X SDS-PAGE sample loading dye before

loading on 15% SDS-PAGE. Samples were subjected to western blot and probed with anti-*Pf*CoSP antibodies. Blots were developed with DAB/H_2O_2 substrate.

Immunofluroscence assays

Thin blood smears of mixed stage *Pf*3D7 cultures at 5% parasitaemia were fixed in methanol for 45 min at −20°C, permeablized with 0.05% PBS/Tween 20, and blocked with 5% (w/v) BSA in PBS. For co-localization studies, mouse anti-*Pf*CoSP (1:250) and rabbit anti-*Pf*NapL (1:250) and rabbit anti-tubulin (1:200) were added as primary antibodies and incubated for 2 h at room temperature. Alexa Fluor 594 conjugated anti-rabbit (1:500, red color, Invitrogen, Carlsbad, CA, USA) and Alexa Fluor 488 conjugated anti-mouse (1:500, green color; Invitrogen) were used as secondary antibodies. The parasite nuclei were counterstained with DAPI (40, 60-diamidino- 2-phenylindole; Invitrogen, USA) and mounted with a coverslip. The slides were examined using a confocal microscope (Olympus, Shinjuku, Tokyo, Japan) with a 100× oil immersion objective.

In vitro antiplasmodial activity of LI71 against human malaria parasite

The antiplasmodial activity of LI71 was tested on *P. falciparum* 3D7 and RKL-9 strain. Different concentration (250, 125, 62.5, 31.25, 15.62, 7.8, 3.9, 1.95 nM) of compound were added in 96-wells flat-bottom microplates in duplicate. Sorbitol synchronized cultures with 0.8–1% parasitemia and 2% hematocrit were dispensed into the plates and incubated for 72 h in a final volume of 100 μL/well. Chloroquine was used as a reference drug. Parasite growth was determined with SYBR Green I based fluorescence assay. Briefly, after 72 h of incubation culture was lysed by freeze-thaw followed by addition of 100 μL of lysis buffer ((20 mM Tris/HCl (Sigma-Aldrich, St. Louis, MO, United States), 5 mM EDTA (Sigma-Aldrich, St. Louis, MO, United States), 0.16% (w/v) saponin (Sigma-Aldrich, St. Louis, MO, United States), 1.6% (v/v) Triton X-(Sigma-Aldrich, St. Louis, MO, United States)) containing 1× SYBR Green I ((Thermo Fisher Scientific, Waltham, Massachusetts, US)). Plates were incubated in the dark at room temperature (RT) for 3–4 h. *P. falciparum* proliferation was assessed by measuring the fluorescence using a Varioskan LUX multimode microplate reader (Thermo Scientific) with an excitation and emission at 485 nm & 530 nm respectively. IC_{50} values were determined via non-linear regression analysis using GraphPad prism 8.0 software. The results were expressed as the percent inhibition compared to the untreated controls and calculated with the following formula: 100× ([OD of Untreated sample – blank]-[OD of treated sample– blank]/[OD – blank]). As blank, uninfected RBCs were used. IC_{50}, which is the dose required to cause 50% inhibition of parasite viability was determined by extrapolation.

Cold shock *P. falciparum* growth assays

Synchronous cultures of *P. falciparum* (3D7) were diluted to 1% parasitaemia and dispensed in 96-well plates along with different concentration of LI71 (250, 125, 62.5, 31.25, 15.62, 7.8, 3.9, 1.95 nM). For cold shock treatment culture were incubated at 25°C for 4 h. Media was exchanged post treatment shock and incubated for 72 h. For control, parasites were left untreated (no drug). SYBR Green-I based fluorescence assay was performed to quantify the parasitemia. IC_{50} values were determined from growth inhibition data using non-linear regression analysis (Prism 8, GraphPad). % Growth was calculated using the formula: (treated/control)×100, and represented as bar graph. All data represent means of results from 3 independent experiments using biological replicates.

Microscopical examination of live/dead staining in malaria parasite

SYTO 9 and propidium iodide staining was performed to distinguish live verses dead parasite at 25°C and 37°C post LI71 treatment. Parasite was treated with and without LI71 at their IC_{50} concentrations (3.968 nM for *Pf*3D7 and 19 nM for RKL-9 at 25°C and 20 nM for *Pf*3D7 and 24.41 nM for RKL-9 at 37°C) at 25°C and 37°C for 4 h at 25°C and 37°C. Post drug washing, culture was kept at 37°C for 68 h. Culture was washed with iRPMI and resuspended in iRPMI. Post 72 h, parasite was stained with SYTO 9 (5 μM) and propidium iodide (30 μM). The slides were examined using a fluorescence microscope (Olympus) with a 100× oil immersion objective.

Estimation of number of transformed *E. coli* cells upon temperature stress

BL21 (DE3) *E. coli* cells transformed with cloned plasmid of *Pf*CoSP was induced with 1 mM IPTG for 4 h and then subjected to temperature stress of 25°C for 8 h. Cultures were taken at 4 h and 8 h post cold treatment and subjected to kanamycin plates at different dilutions. Plates were kept at 37°C overnight.

P. falciparum gametocyte culture and gametocytogenesis

The strains of RKL-9 of*P. falciparum* were cultured *in vitro*.[52] Here parasites were maintained in human type O positive RBCs at 5% haematocrit (HCT) in RPMI 1640 medium containing 2 g/L sodium bicarbonate, 50 mg/L hypoxanthine (Sigma-Aldrich, St. Louis, MO, United States) with the addition of 10% (v/v) naturally clotted heat-inactivated O+ human serum. The cultures were maintained at 37°C in a standard gas mixture consisting of (5% O_2, 5% CO_2, and 90% N_2). To trigger gametocytogenesis, 10 mL cultures were diluted to 0.5% parasitaemia at 5% HCT. Media was changed daily for 3 days until 5% parasitaemia was reached. At this point the HCT was lowered to 2.5% and the culture was treated for 48–72 h with 50 mM N-acetylglucosamine (NAG; Sigma-Aldrich) in order to clear residual asexual parasites and obtain a virtually pure gametocyte culture, typically containing 2–4 gametocytes/100 RBCs at late stage II to early stage III of maturation.

Gametocyte maturation in microwell plates

To analyze gametocyte development in 96-well plates, asexual parasite cultures were synchronized by purifying schizonts percoll gradient-centrifugation and allowed to reinvade erythrocytes. After two rounds of reinvasion, the cultures were treated with NAG (50 mM) for 72 h in order to clear residual asexual parasites and obtain a virtually pure gametocyte culture. Aliquots of 100 μL of synchronized gametocyte culture (typically at ~2% gametocytaemia), diluted to 1% HCT, were seeded in 96-well flat-bottomed plates in presence of LI71 at 10, 50, 100, 250 and 500 nM concentration respectively. Gametocytes were left untreated as control. Media with appropriate concentration of LI71 was exchanged daily for continuous 12 days. Giemsa-stained blood smears were observed to see the effect of LI71 on gametocyte development.

Effect of L171 on *P. falciparum* exflagellation *in vitro*

To study the effect of LI71 on *P. falciparum* male gametocyte ex-flagellation, stage V gametocytes were treated for 30 min with 10, 50, 100, 250 and 500 nM of LI71. Infected RBCs were left untreated as control. Samples were kept at 37°C and incubated for 1 h. After incubation compound treated samples were washed and mixed immediately with 200 μL of ex-flagellation medium (RPMI1640 containing 25 mM HEPES, 20% FBS, 10 mM sodium bicarbonate and 50 mM xanthurenic acid at pH 7.4) and kept at 24°C for 15 min. Ex-flagellation centers were then counted in 10–12 field using 40× objective of Fluorescence microscope.

qRT-PCR for gene expression analysis

Total RNA from *P. falciparum* infected erythrocytes treated with and without LI71 (1.35 nM;1x IC_{50}, 13.5 nM; 10x IC_{50} and 1 μM; 740.74x IC_{50}) for 6 h were isolated using the TRIZOL reagent (Invitrogen, Grand Island, NY) and its concentration was quantified using a Nanodrop ND-1000 spectrophotometer (Thermo Fischer, USA). *P. falciparum* infected erythrocytes were also treated with SAHA (5 μM) alone, and combination of LI71 (1.35 nM; 1x IC_{50}) and SAHA (5 μM) for 6 h to assess the combined effect of both drugs. cDNA was prepared from two micrograms of RNase-free DNase treated total RNA using first-strand cDNA Synthesis Kit (Applied Biosystems), as per manufacturer's instructions, using random hexamer primers. PCR reactions were carried in Applied Biosystems, Real-Time PCR System (ABI, CA, USA) using PowerUp SYBR Green PCR Master Mix (Applied Biosystems). The detail of the primers (sequences and annealing temperatures) used is given in Figure S8. Thermal profile for the real-time PCR was amplification at 50°C for 2 min followed by 40 cycles at 95°C for 15 s, 60°C for 30 s and 72°C for 1 min. Melting curves were generated along with the mean C_T values and confirmed the generation of a specific PCR product. Amplification of 18S was used as internal control for normalization. The results were expressed as fold change of control (Untreated samples (18S)) using the $2^{-\Delta\Delta CT}$ method. Each experiment was done in triplicates and repeated three times. Statistical significance was determined by Student's t-test analysis ($p < 0.05$). Percentage change in expression levels were calculated as (LI71+ SAHA/SAHA) ×100 where both drugs were used for treatment.

QUANTIFICATION AND STATISTICAL ANALYSIS

All the data and the fold-expression (qRT-PCR analysis) are shown as mean ± SD. Statistical differences were determined using Student's unpaired 2-tailed t-test. All statistics were performed using GraphPad Prism Version 8.0 (GraphPad Software, USA). $p \leq 0.05$ was considered significant.